RESULTS OF COMPREHENSIVE STCM DATA FUSION EXPERIMENT

Oltrogge, D.L.[1], Wauthier, P.[2], Vallado, D.A.[1], Alfano, S.[1], Kelso, T.S.[1]

[1] COMSPOC Corporation, 7150 Campus Dr. Ste 260, Colorado Springs CO 80920 USA, Email: cssi@comspoc.com
[2] SDA Executive Director, Château de Betzdorf, Betzdorf 6815. Luxembourg, Email: Pascal.Wauthier@ses.com

ABSTRACT

This paper documents the findings of a demonstration of the benefits of multi-source data fusion and advanced analytics to achieving accurate Space Situational Awareness (SSA) for the Space Traffic Coordination and Management (STCM) mission. After extensive testing and statistical assessments of predictive positional accuracy for seventeen spacecraft spanning LEO, MEO and GEO orbit regimes, the team found that fusing government, commercial, and satellite operator data with advanced data processing techniques results is essential to enabling comprehensive, timely, and accurate collision avoidance services for all satellite operators.

In this assessment of spacecraft positional accuracy, which was conducted between 15 and 30 September 2020, the team was able to "crowd source" data from SSA data providers (e.g., radar or optical sensor information), government and satellite operators to typically improve SSA accuracy by ten to fifty percent in LEO and a factor of ten or more in GEO, thereby dramatically improving flight safety.

1 Introduction

There have been numerous, lengthy discussions on the need for Space Traffic Coordination (STC) and Space Traffic Management (STM), including nuanced discussions on the lack of consensus of how these terms are defined. Despite these efforts, there has been a conspicuous void in understanding what the requirements are for the underlying Space Situational Awareness (SSA) system and demonstrating how well current legacy SSA and commercial SSA/data fusion systems can meet those requirements.

2 STCM data fusion experiment

To address this void, a coalition of willing government and commercial SSA providers and spacecraft operators resolved to conduct a comprehensive two-week data fusion experiment which combined observational and operations data from all factions. The STCM demonstration itself was originally to be composed of two campaigns, each designed to help us explore, for a small but orbit-diverse set of operational spacecraft, the operational challenges and solution trade space associated with flight safety and space traffic coordination and management. An overview of each campaign is provided in the sections below.

2.1 STCM data fusion schedule

This demonstration occurred during the month of September 2020. The overall schedule was:

22 Aug 2020	Complete invitation calls to demonstration participants
27 Aug to 14 Sep 2020	Data flow to COMSPOC from SDC, operators, SSA systems
15 – 30 Sep 2020	Comprehensive data fusion, solve accurate orbits, infuse those orbits back into the SDC for comparative SSA, show how this impacts/influences flight safety
21 Oct 2020	Initial presentation at STCM Special Session of AIAA ASCEND Conference

2.2 STCM Campaign #1: Positional accuracy via data fusion and analytics

In our first campaign of this STCM demonstration, the STCM consortium demonstrated the utility of comprehensive data fusion across multiple data sources and data types and quantified its benefits to orbit solution timeliness, historical and predictive positional accuracy, completeness, transparency, and comparative SSA.

2.3 STCM Campaign #2: Comparative SSA and flight safety improvements

In the second STCM campaign, the STCM consortium explored the benefit to safety of flight of comprehensively gathering and fusing space data across multiple data sources and data types and of comparative SSA assessments.

Due to a lack of close approaches for the seventeen selected spacecraft during this time period, samples of typical Comparative SSA Analyses were provided to give the reader a sense for how such comparisons aid the operator in decision making for safety of flight,

Proc. 8th European Conference on Space Debris (virtual), Darmstadt, Germany, 20–23 April 2021, published by the ESA Space Debris Office
Ed. T. Flohrer, S. Lemmens & F. Schmitz, (http://conference.sdo.esoc.esa.int, May 2021)

examining all possible combinations of positional data products and their precision, including operator predictive ephemerides, fused orbit solution ephemerides (smoothed and predicted for 7 days) and forward predictions, and SP and TLE products, using existing SDC Comparative SSA tools and processes.

2.4 STCM demonstration participants

The consortium of fourteen government, space operators, academia and SSA service entities participating in this STCM demonstration, contributing ephemerides, maneuver plans, observations, and sponsorship, included:

Who	Eph	Obs	Mnvr Plans	Analysis	Sponsor
Office of Space Commerce				✓	✓
US Space Command and 18th Space Control Squadron		✓			
Commercial Space Operations Center (COMSPOC)	✓	✓			
Kratos		✓			
Raytheon		✓			
Rincon		✓			
Thoth (ARO)		✓			
Iridium	✓	✓	✓		
NOAA	✓	✓	✓		
Planet	✓	✓	✓		
SES	✓	✓	✓		
Telesat	✓	✓	✓		
Univ. of Texas/Austin				✓	✓
Space Data Association (SDA)				✓	✓

2.5 Spacecraft selected for this demonstration

For this demonstration, seventeen spacecraft were selected as shown in ***Fig. 1*** and detailed in *Table 1*. Operator estimates of thruster configuration, manoeuvrability, conjunction rates and approximate number of annual collision avoidance actions taken are also listed in *Table 1* when provided by the operator.

The observational data available for each spacecraft are provided in *Table 2*.

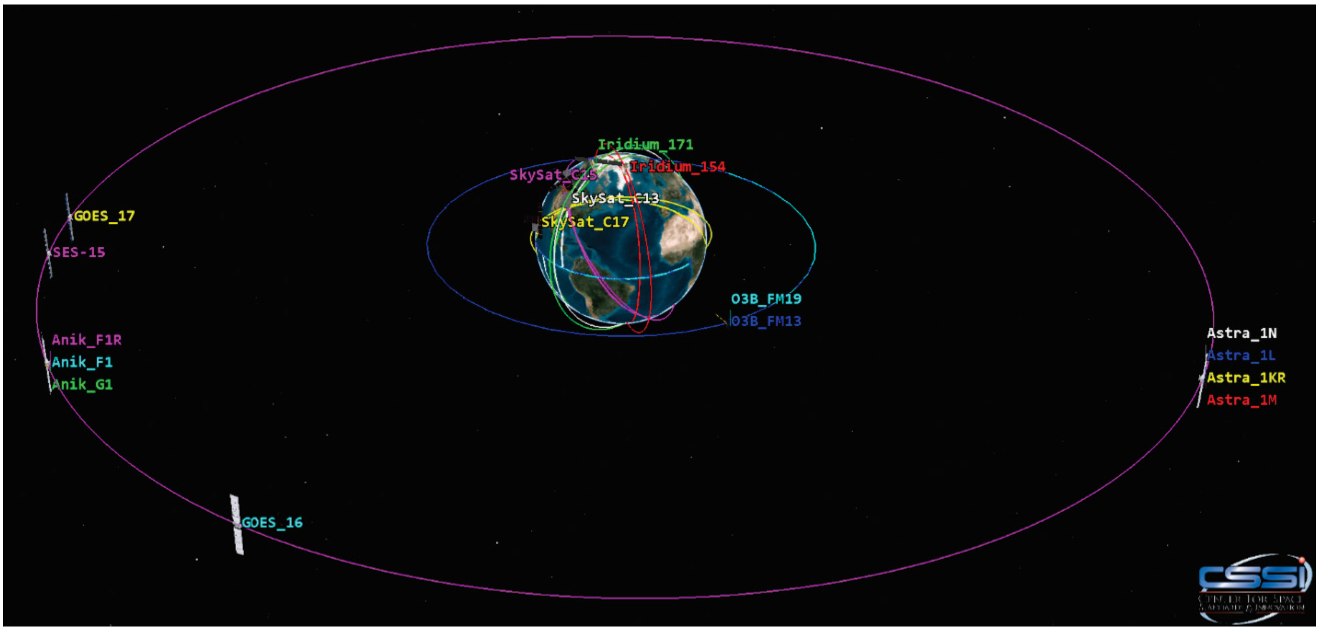

Fig. 1 Depiction of 10 GEO, 2 MEO and 5 LEO spacecraft included in demonstration.

Table 1 Seventeen spacecraft incorporated into STCM demonstration.

Operator	S/C name	SSC	Thruster Technology	Thruster config (e.g., 4x1N)	Isp (s)	ΔV Range (m/s)?	Est. conjunctions/yr.	Est. avoidance actions/yr.*
NOAA	GOES 16	41866						
	GOES 17	43226						
SES	ASTRA 1KR	29055	Monoprop + Arc jet	~1N	200 to 480 sec	~1 m/s maneuver average	~300 (all 53 SES GEO satellites)	~10 (all 53 SES GEO satellites)
	ASTRA 1L	31306	Monoprop+ Arc jet	~1N	200 to 480 sec	~1 m/s maneuver average	~300 (all 53 SES GEO satellites)	~10 (all 53 SES GEO satellites)
	ASTRA 1M	33436	Biprop	~7N	230 to 270 sec	~1 m/s (maneuver average)	~300 (all 53 SES GEO satellites)	~10 (all 53 SES GEO satellites)
	ASTRA 1N	37775	Biprop	~7N	230 to 270 sec	~1 m/s (maneuver average)	~300 (all 53 SES GEO satellites)	~10 (all 53 SES GEO satellites)
	SES-15	42709	Ion	~0.04N	Up to 3400 sec	~0.08 (maneuver average)	~300 (all 53 SES GEO S/C)	~10 (all 53 SES GEO satellites)
	O3B FM13	43234	Monoprop	~4N	~230 sec	~0.8 ms (maneuver average)	~30 (all 20 O3b)	0 to 1 (all 20 O3b satellites)
	O3B FM19	44113	Monoprop	~4N	~230 sec	~0.8 ms (maneuver average)	~30 (all 20 O3b)	0 to 1 (all 20 O3b satellites)
Planet	SkySat-C13	43802	HPGP	4x1N	230	0.1-5	5-10	0-3
	SkySat-C15	45790	HPGP	4x1N	230	0.1-5	5-10	0-3
	SkySat-C17	46179	HPGP	4x1N	230	0.1-5	5-10	0-3
Telesat	Anik F1	26624	Chemical + Ion				120	6
	Anik F1R	28868	Chemical				120	6
	Anik G1	39127	Chemical				120	6
Iridium	Iridium 154	43574	Chemical	4x1N prograde, 1x1N retrograde, All pulsed	140,177	+.00089 to +.05, -0.00023 to -0.05, (stationkeep)	1 requiring mitigation	31
	Iridium 171	43929	Chemical	4x1N prograde,1x1N retrograde, All pulsed	140,177	+.00089 to +.05, -0.00023 to -0.05 (stationkeep)	1 requiring mitigation	31

*(including modifications to stationkeeping maneuver duration and/or timing for the purpose of avoiding collision)

Table 2 Observations, closest approaches and metadata for these spacecraft.

Operator	S/C name	SSC	WAAS Ephemeris?	SDA Participant?	GPS NavSol	Active ranging	Operator Passive RF	SSA Passive RF	Optical Tracking	Radar Tracking	Orbit during demo or longitude if GEO)	Closest Approach during demo: SSC/Time UTC/ Distance(km)
NOAA	GOES 16	41866		●	●				●	●	75° W	N/A
	GOES 17	43226		●	●				●	●	75° W	12996 on 19 Sep at 17:21/21.909
SES	ASTRA 1KR	29055		●			●		●		19.2° E	27168 on 28 Sep at 12:18/33.902
	ASTRA 1L	31306		●			●		●		19.2° E	27168 on 28 Sep at 12:19/25.944
	ASTRA 1M	33436		●		●	●		●		19.2° E	27168 on 29 Sep at 00:16/15.903
	ASTRA 1N	37775		●		●	●		●		19.2° E	27168 on 29 Sep at 00:16/36.119
	SES-15	42709	●	●		●	●		●	●	129° W	N/A
	O3B FM13	43234		●	●				●	●	Eq. circ. 8,000 km	38996 on 28 Sep at 18:18/29.837
	O3B FM19	44113		●	●				●	●	Eq. circ. 8,000 km	38996 on 28 Sep at 13:01/26.830
Planet	SkySat-C13	43802		●	●					●	Sun-sync, 450 km	16865 on 27 Sep at 00:53/2.249
	SkySat-C15	45790		●	●					●	Sun-sync, 400 km	N/A
	SkySat-C17	46179		●	●					●	212x365 km, orbit-raising to 400 km	N/A
Telesat	Anik F1	26624		●		●		●	●	●	107.3° W	28659on 17 Sep at 01:41/33.180
	Anik F1R	28868	●	●		●		●	●	●	107.3° W	28659 on 17 Sep at 03:07/45.307
Telesat	Anik G1	39127		●		●		●	●	●	107.3° W	28659 on 17 Sep at 02:08/19.871
Iridium	Iridium 154	43574		●		●				●	780 km circ. at 86.4°	N/A
	Iridium 171	43929		●		●				●	780 km circ. at 86.4°	25417 on 30 Sep at 18:02/2.893

The SSA systems incorporated into this comprehensive data fusion demonstration are listed in *Table 3*.

Table 3 SSA observation types by contributing SSA organization.

Organization	Radar	Ground-based Optical	Space-based Optical	Passive RF	Data fusion, analytics
Thoth	●				
COMSPOC		●			●
Kratos				●	
Raytheon	●				
Rincon				●	
Space Surveillance Network	●	●	●		

3 Assessing SSA positional accuracy requirements

It is worth pausing at this stage to consider what requirements our SSA system is trying to fulfil. From a flight safety standpoint, there exist a wide variety of conjunction assessment screening metrics. The choice of metric often depends on the orbit regime and its associated threat profile, operator staffing, maneuver prolusion capability and resources, etc. For any such conjunction assessment metric to be operationally relevant and viable, the accuracy of SSA data must be sufficient to support the selected collision avoidance maneuver "Go-No Go" threshold. In this section, we will demonstrate how to map the user's chosen threshold into derived accuracy requirements for each of the conjuncting pair of objects using one of the most embraced metrics (collision probability or Pc) and one of the most used Pc thresholds of one-in-ten thousand.

Just to again note, there are many metrics, or even combinations of metrics, being operationally used today. These metrics will have diverse ways of determining what accuracy is required to support a chosen conjunction metric threshold value. But like the process shown below, it is incumbent upon each operator to ascertain what accuracy the SSA data needs to have to ensure that their flight safety processes are operationally relevant and effective.

3.1 SSA positional accuracy requirements corresponding to Pc thresholds

The relationship between absolute maximum probability $\boldsymbol{P_{max}}$ for spherical objects and miss distance $\boldsymbol{d}$ can be approximated if the Combined Hard Body Radius $\boldsymbol{CHBR}$ and covariance aspect ratio $\boldsymbol{AR}$ are known[1]. $\boldsymbol{AR}$ is the ratio of the covariance major axis to its minor axis in the encounter plane. The equations are:

$$P_{max} \cong \left(\frac{\alpha}{1+\alpha}\right)\left(\frac{1}{1+\alpha}\right)^{\frac{1}{\alpha}} \qquad (1)$$

$$\alpha = \frac{CHBR^{\,2} AR}{d^2} \qquad (AR \geq 1) \qquad (2)$$

To provide insight into these relationships, we use the above equations to create nomograms as provided in **Fig. 2** and **Fig. 3**. A nomogram or nomograph is a chart usually consisting of three or more sets of data. Knowing any two sets of data allows the user to find the value for the other, unknown, corresponding value(s). They are simply graphical calculating devices designed to allow the approximate computation of a function[2]. Its name is derived from the Greek νόμος (nomos) meaning "law," and γραμμή (grammē) meaning "line." Nomographs are simply "lines that follow laws."

With these nomograms, it is not necessary for the user to solve algebraic equations, to look up values in data tables and possibly interpolate those values, or to use a calculator to obtain results. The user need not even have knowledge of the fundamental equation(s) or principle(s) represented. Typically, a sharp pencil and keen eye will produce results within 5% of an exact numerical solution.

To facilitate nomogram creation, we introduce the intermediate variable $\boldsymbol{\beta}$ such that:

$$\beta = \frac{AR}{d^2} \quad (3)$$

The purpose of the intermediate variable $\boldsymbol{\beta}$ is simply to link two nomograms such that the three inputs P_{max}, $CHBR$, and AR produce d as shown in **Fig. 2**. For this example, we use a P_{max} value of 1.0x10^{-4}, a $\boldsymbol{CHBR}$ of 5 meters, and a covariance aspect ratio AR of 3 to obtain a miss distance d of 525 meters.

The major-axis standard deviation σ_{major} associated with P_{max} is found through the equations:

$$\sigma_{major} = \sqrt{\frac{-\eta}{2 \cdot ln\left(\frac{d^2}{d^2+\eta}\right)}} \quad (AR \geq 1) \quad (4)$$

$$\eta = AR \cdot CHBR^{\,2} \,. \qquad (5)$$

From the depiction of these relationships in **Fig. 3,** one can then determine that a miss distance $\boldsymbol{d}$ of 525 meters for this example results in a combined major-axis standard deviation $\boldsymbol{\sigma_{major}}$ of 371m.

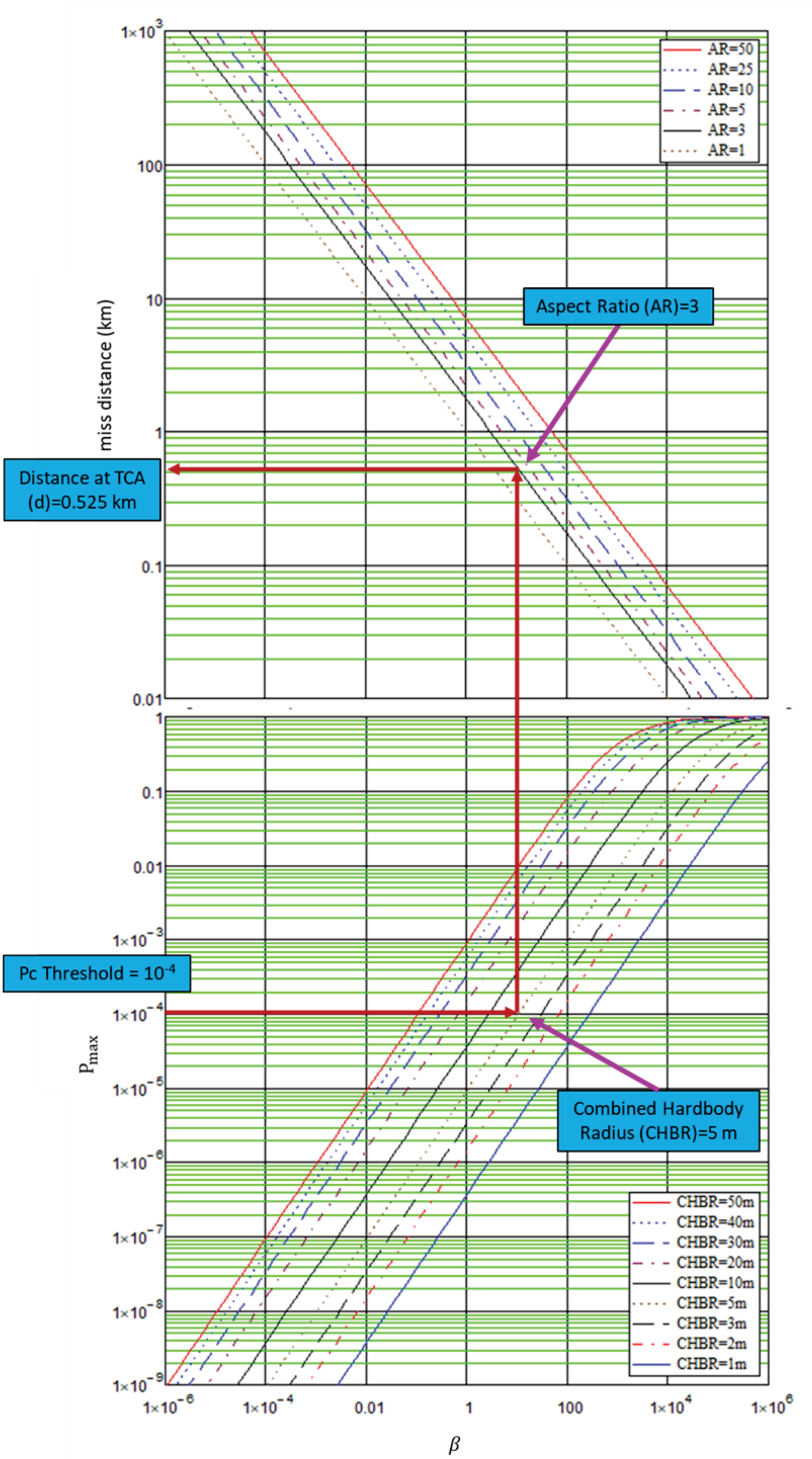

Fig. 2 Example of using nomograms to determine distance d from P_{max}, CHBR, and AR.

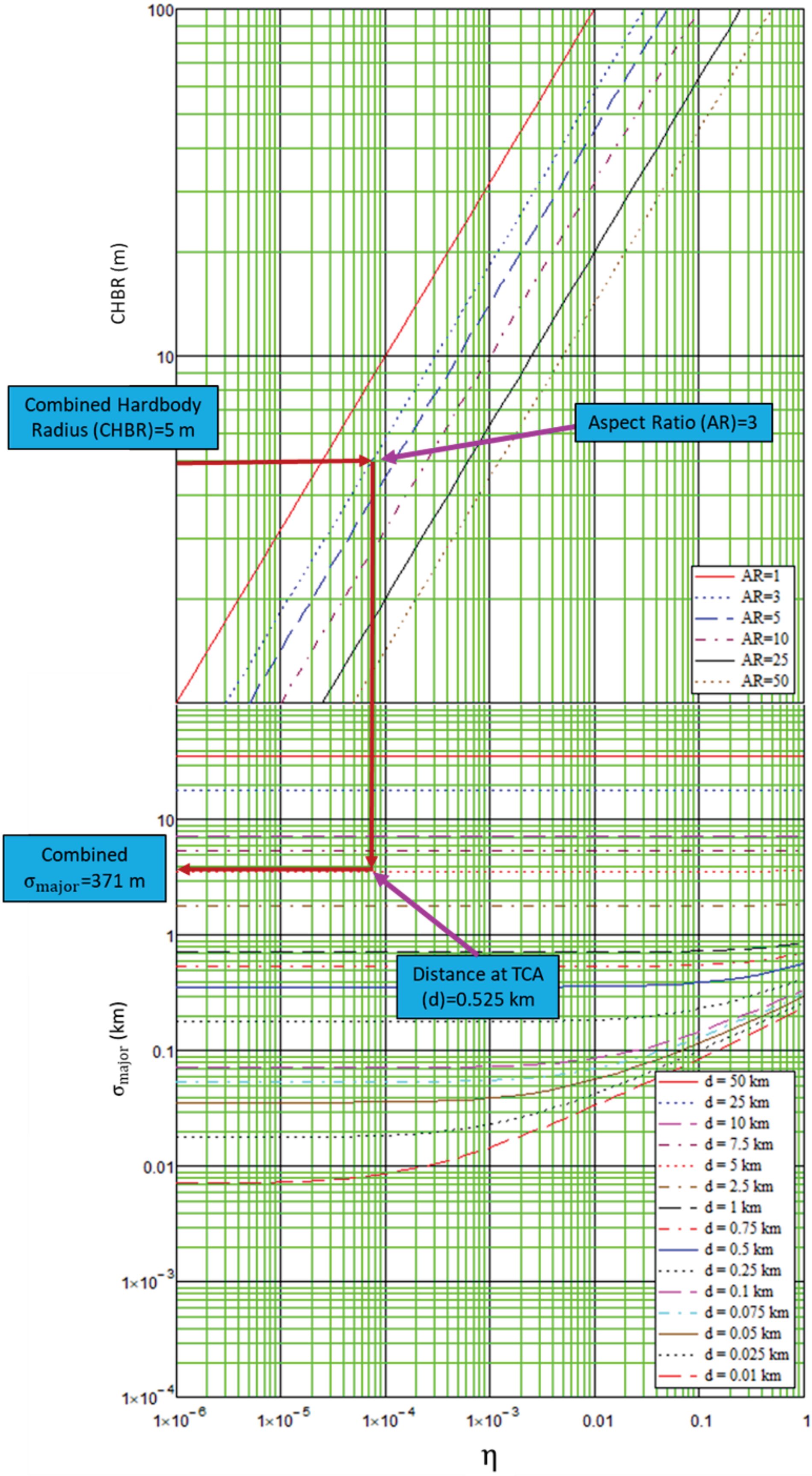

Fig. 3 Example of using nomograms to determine σ_{major} from r, d, and AR.

Table 4. Maximum allowable one-sigma error ellipsoid dispersion for assorted combinations of maximum probability and CHBR for aspect ratio AR=3.

Pmax	CHBR (m)	AR	distance (m)	combined sigma major (m)	individual sigma major (m)
1.E-04	0.5	3	53	37	26
1.E-04	1	3	105	74	53
1.E-04	1.5	3	158	111	79
1.E-04	5	3	525	**371**	263
1.E-04	10	3	1050	743	525
1.E-04	20	3	2101	1486	1051
1.E-04	50	3	5252	3714	2624
5.E-04	0.5	3	24	17	12
5.E-04	1	3	47	33	24
5.E-04	1.5	3	70	50	35
5.E-04	5	3	235	166	117
5.E-04	10	3	470	332	235
5.E-04	20	3	939	665	470
5.E-04	50	3	2348	1661	1174
1.E-03	0.5	3	17	12	8
1.E-03	1	3	33	24	17
1.E-03	1.5	3	50	35	25
1.E-03	5	3	166	117	83
1.E-03	10	3	332	235	166
1.E-03	20	3	664	470	332
1.E-03	50	3	1659	1174	830

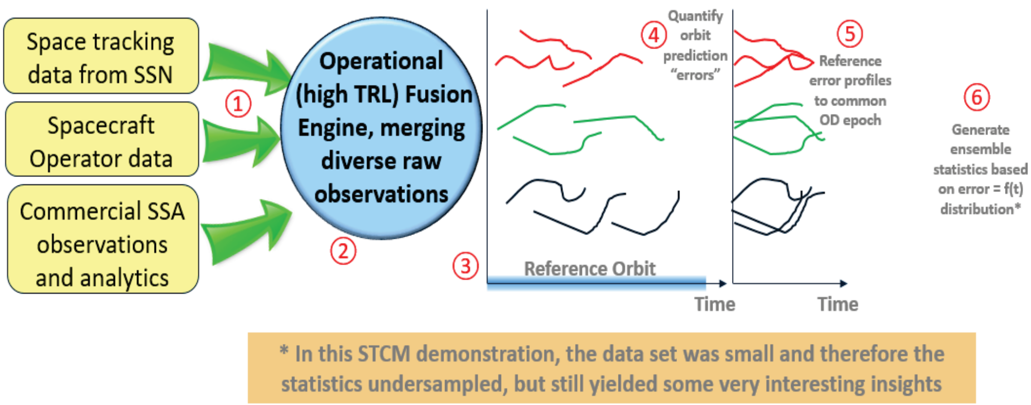

Fig. 4 Data fusion and accuracy assessment analysis steps.

The combined σ_{major} value obtained from the nomograms above can be statistically divided amongst both objects in some manner. Since debris does not maneuver and apart from High Area to Mass Ratio (HAMR) objects is generally well-behaved in terms of propagation, one could conceivably require the orbital debris object's positional accuracy to be higher than the accuracy required of an active spacecraft. But given that debris can be much smaller (and therefore harder to detect, track and maintain custody of), the remainder of this paper assumes that the positional accuracy "allocation" corresponding to a specified Pc threshold is divided equally amongst both the primary and secondary (typically debris) objects.

Another important consideration is how to relate "maximum probability" with the Pc threshold used by the operator. By definition, "maximum probability" means the highest Pc value that could ever, in just the ideal circumstances, result from a given conjunction condition. Obviously, to only have SSA data that is only just barely accurate enough to yield, in a very rare case, a collision probability that only matches (but cannot exceed) the operator's selected collision probability threshold is insufficient; the operator might as well not monitor collision probability in that case. Instead, it was (somewhat arbitrarily) assumed for the remainder of this paper that **for a collision probability threshold metric to be operationally relevant and effective, the accuracy of the underlying SSA positional data must be capable of yielding Pc values that are a factor of five larger than the user's selected Pc threshold**.

Table 4 provides required accuracies associates with common conjunction screening values, produced using the exact relationships and equations. Note that for a typical Low Earth Orbit (LEO) Combined Hard Body Radius (CHBR) of 1 meter, an operator's Pc threshold of one in ten thousand maps to a P_{max} of five in ten thousand and an individual allowable major eigenvalue's corresponding one-sigma accuracy of no greater than 24 meters, whereas in Geosynchronous Earth Orbit (GEO) the typically larger spacecraft might yield an allowable one-sigma accuracy of no worse than 117 meters. These are very demanding requirements indeed!

4 STCM data fusion accuracy demonstration

Now that a sample SSA accuracy requirement has been selected, we can now resume discussion of the STCM data fusion and accuracy assessment campaign. The analysis process consisted of the six steps shown in **Fig. 4**. In Step 1, we collected disparate, diverse data from the SSN, from spacecraft operators, and from commercial SSA providers, ingest these raw measurements into a single comprehensive and technically mature data fusion engine. In Step 2, we developed accurate reference orbits for each space object participating in the demonstration. In Step 3 and 4, we gathered and differenced all orbit positional knowledge products with respect to the reference orbit as a function of time. In Step 5, we re-baseline all positional knowledge products to a common "time since OD epoch." And finally, in Step 6 we generated accuracy distribution statistics.

Data fusion is a complex topic that involves many factors. In Chapter 10 of [3], the overall topic of orbit determination is discussed. Many of the factors involved in data fusion are discussed in Sec 10.9 (Practical Considerations). The discussion goes through observation data, availability, quantity, location of observations, types of data, and observability considerations and how they apply to the overall OD accuracy.

Prior to providing the results from this demonstration, it is important to note that the fourteen participating organizations, spanning government and commercial arenas, did so with the goal of demonstrating the power of data fusion, and not in diminishing the value of any SSA product. These products all contribute to flight safety, sustainability, and operations. Overall, we found (as shown in Section 9) that comprehensive data fusion using a diverse set of tracking sensors coupled with advanced analytics yielded a ten to fifty percent improvement in positional accuracy and timeliness in LEO, and a more than ten-fold improvement in GEO.

5 Reference orbit development and accuracy

Absolute positional accuracy of SSA products can be assessed once one has access to an accurate "truth" (or nearly so) reference orbit. The STCM demonstration included the generation of high-accuracy reference ephemerides (step 3 in **Fig. 4**) based upon GPS Navigation Solution (NavSol) data, Wide Area Augmentation System (WAAS) data, passive Radio Frequency (RF) observations, and data-rich tracking observations from numerous, diverse sensors.

It is important to characterize the estimated accuracy of such reference orbits. The higher accuracy reference orbits are based upon laser ranging, WAAS, GPS and passive RF data. A characterization of the major and minor 2σ error range for a GEO reference orbit is shown in **Fig. 5**, which indicates that the 2σ positional knowledge associated with this particular reference ephemeris ranges between 25 and 120 meters, which means that the error is usually below these limits (and typically, well below, such that more than 70% of the time the accuracy is perhaps 40 meters or better when averaged across the two-week STCM demo period and across all viewing orientations). These reference orbits provide a statistically significant set of "truth" data that can be used to conduct positional error assessments (as presented in the next section).

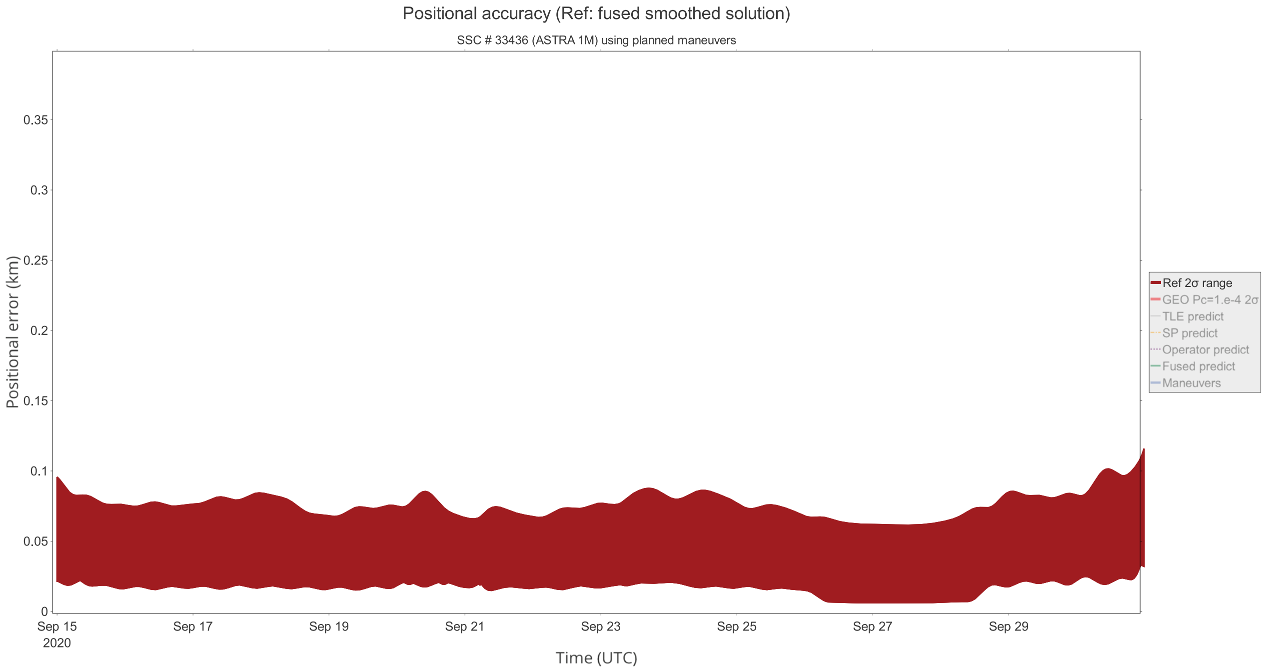

Fig. 5 Reference orbit major and minor eigenvalue-based 2-sigma boundaries (in red).

6 SSA data types evaluated

Five SSA/orbit prediction sources were analyzed in this STCM data fusion demonstration. They are:

- Two-Line Element sets (or TLEs) which are based on optical and radar but have no planned maneuvers or other data sources incorporated.
- Special Perturbations (SP) ephemerides that use a higher fidelity propagator but are otherwise based upon the same observational data as TLEs (again typically without planned maneuvers).
- Spacecraft operators' ephemerides, which typically draw from a more diverse set of observation types, with some operators combining their ranging measurements with passive RF, GPS (navigation solution or NavSol), and even optical measurements with their planned maneuvers.
- The fused orbit solution incorporated optical, radar, active ranging, passive RF, and planned maneuvers. Note that while NavSol could also have been incorporated into the fused solution, for this demonstration we chose to show that even without GPS NavSol data, the application of large-scale data fusion, advanced analytics and comprehensive data exchange are necessary to meet obtain the high-accuracy SSA data needed for flight safety.
- NavSol ephemerides, from which orbits were estimated by the STCM demonstration team.

7 Assessing TLE, SP, operator, GPS and fused positional accuracy

With such reference orbits in hand, the accuracy (i.e., positional error) of a variety of SSA and orbit products is shown in **Fig. 6** and **Fig. 7**, corresponding to Step 4 in **Fig. 4**. The smaller the positional error, the better the STCM accuracy will be, and the more actionable and effective the result.

Many accuracy and covariance realism results were generated stemming from this single two-week demonstration. As these results are voluminous, they have been placed in Appendix 1 through Appendix 4.

In this section, we want to familiarize the reader with the overall format of the accuracy plot (see **Fig. 6**) format adopted for characterizing accuracy of all seventeen LEO, MEO and GEO spacecraft participating in the demonstration. The plot characterizes the positional error associated with a variety of SSA positional products shown in the legend at right, with TLEs (in white), SP ephemerides (in orange), operator ephemerides (in purple), fused solutions (in green), and where present, GPS-based NavSol solutions (in blue).

We first define the axes of this accuracy plot, with the x-axis representing the date and the y-axis representing positional error in kilometers. The horizontal red line just barely visible at the bottom of the graph represents the accuracy required to operationally use a Pc threshold of one in ten thousand as a conjunction screening threshold (as derived in Section 3).

The vertical blue lines depict when the spacecraft performed a maneuver, with the thickness of the maneuver bar scaled to reflect its duration. In this study, we examined the use of operator-provided maneuver plans (when available) as well as our COMSPOC non-cooperatively determined (“Determined”) maneuvers.

Against this backdrop, we can see how the sequence of TLEs (depicted as thin black lines) propagates forward and the error associated with each TLE as a function of time. The orbit epoch for each TLE is represented by the up-pointing triangle at the beginning of each line. You can see that the TLE accuracy typically ranges between one and five kilometers for this spacecraft during this two-week demonstration period. But you can also see that the maneuvers conducted by the spacecraft on 20 and 23 September introduced oscillating and secular degradations respectively in predictive accuracy. This degradation is to be expected, as the TLE prediction does not reflect planned maneuvers.

Next, we examine how Special Perturbations (SP) ephemerides (depicted as dotted orange lines) performs during this same period. You can see that while SP typically has significantly better accuracy than TLEs most of the time for this spacecraft, it frequently exceeds the allowable error. Also notice that the same maneuvers that caused the TLE accuracy to degrade equally impacted SP accuracy - - which is to say that for unmodeled forces such as this maneuver, TLE and SP accuracy are affected equally, despite the innate higher fidelity of SP perturbations theory. In fact, one interesting observation, consistent with prior operational experience, is that while SP is typically more accurate than TLE solutions in the short-term, TLE accuracy can often match and even improve upon SP accuracy over propagation timespans of one to two days or more.

But this brings us to about the limit of what can be gleaned from this plot using this y-axis scale, because the area of high interest in the vicinity of or below the Pc threshold-derived accuracy constraint is simply too compressed to be visible on this linear scale.

While one could repeatedly zoom in on the y-axis to gain clarity in this accuracy depiction at higher fidelity levels, we chose instead to employ a logarithmic y-axis scale as shown in **Fig. 7**. But this switch must be accompanied by a caution: **a log scale tends to downplay large positional errors while amplifying small errors. Note that the green line spans a factor of 1,000! - - so user beware**.

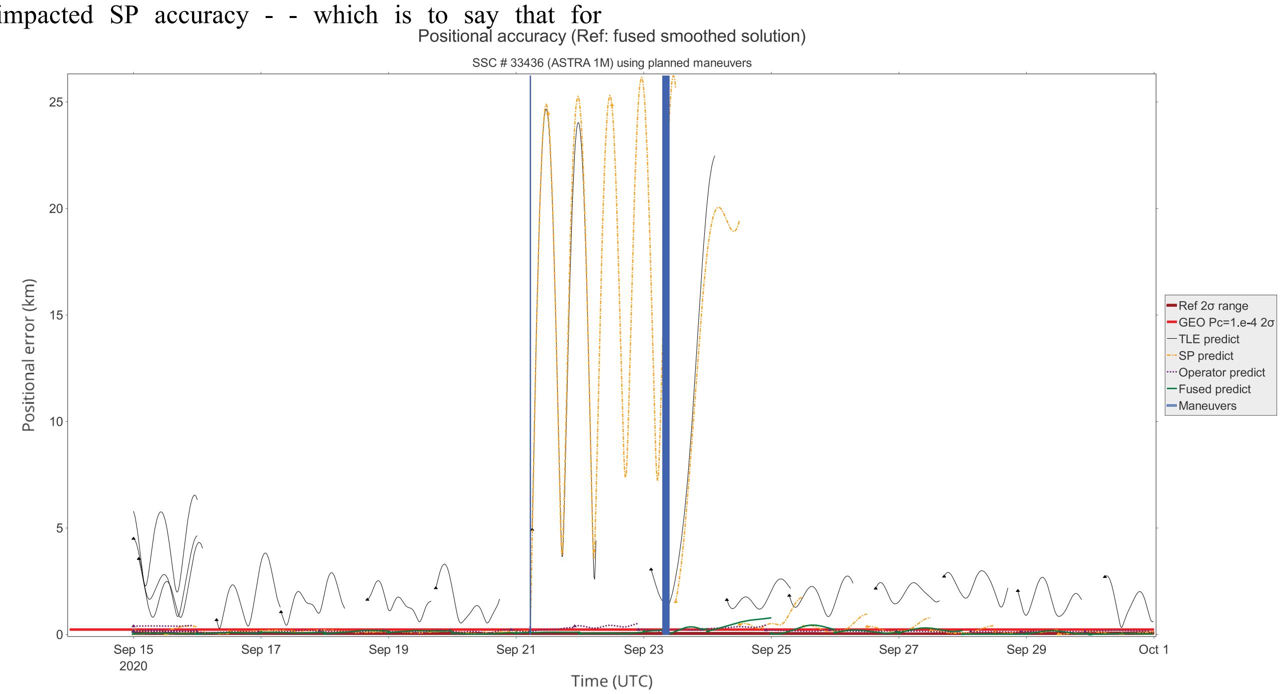

Fig. 6 Example of STCM demonstration predict accuracy on a linear y-axis scale.

Using the log scale, the operator’s ephemerides (dotted purple) and the STCM demonstration’s Fused Solution are clearly visible. In this case, it appears that while the planned maneuver was incorporated into the fused orbit prediction, it either was not well-calibrated or could be further improved upon, as some error was still introduced by the second maneuver event.

And finally, we can add the reference orbit’s 2σ error ranges from **Fig. 5** to obtain the full (and “busy”) accuracy plot format as shown in **Fig. 8**.

Again, the full set of accuracy results for these seventeen spacecraft during this two-week STCM demonstration are provided using spacecraft operator-provided maneuver plan data in Appendix 1, and in Appendix 2 in cases where maneuvers were non-cooperatively refined or determined by the COMSPOC).

As another example, the degradation in ANIK G1 positional accuracy of the fused solution caused by a maneuver on 17 September (**Fig. 9**) was addressed by non-cooperatively solving for that maneuver (**Fig. 10**).

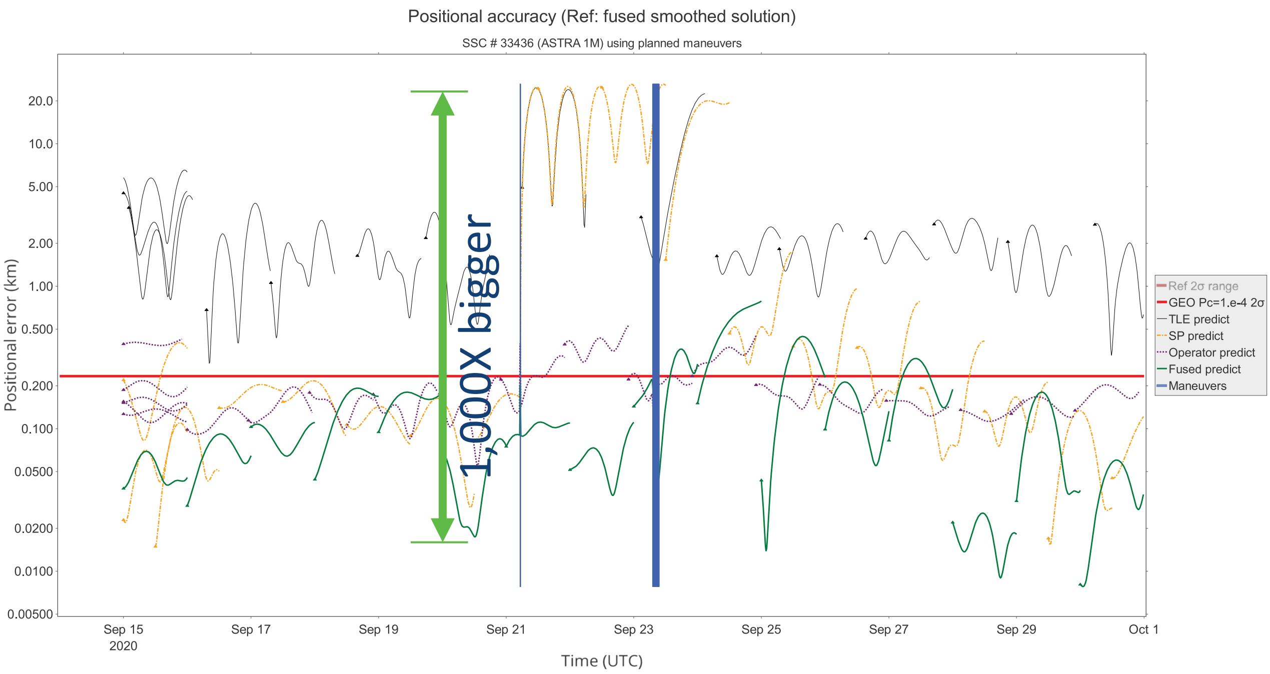

Fig. 7 Example of STCM demonstration predict accuracy on a logarithmic y-axis scale.

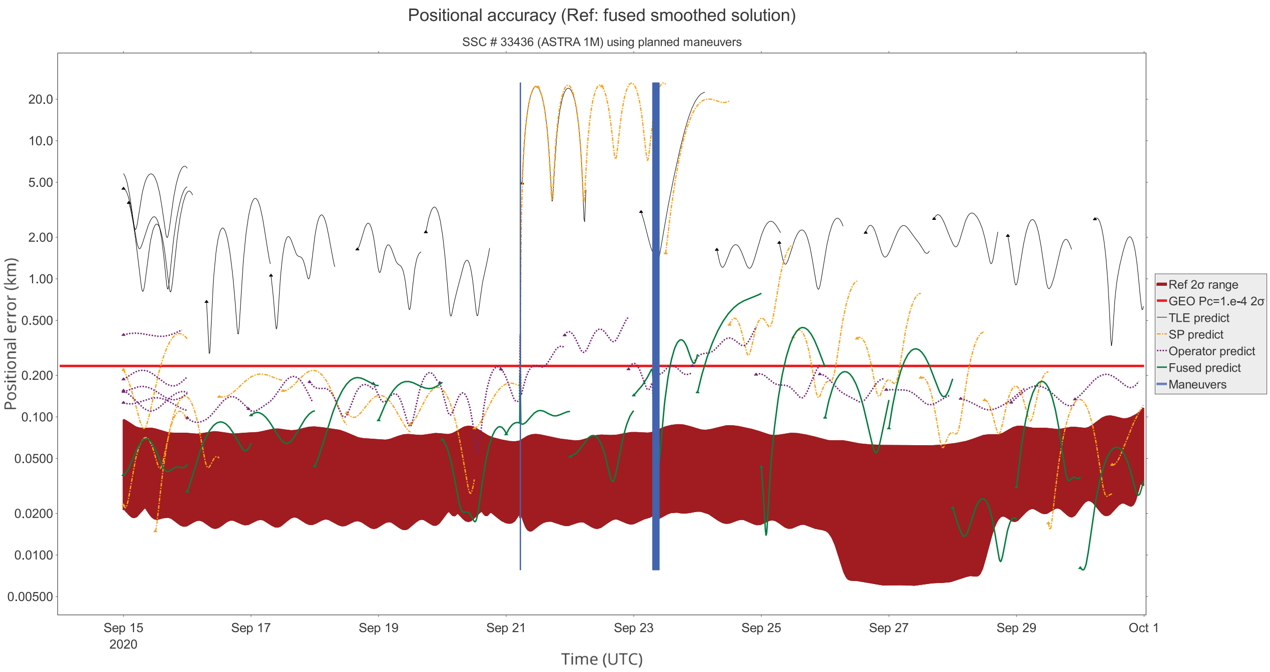

Fig. 8 Complete format including major and minor eigenvalue 2-sigma range (in red).

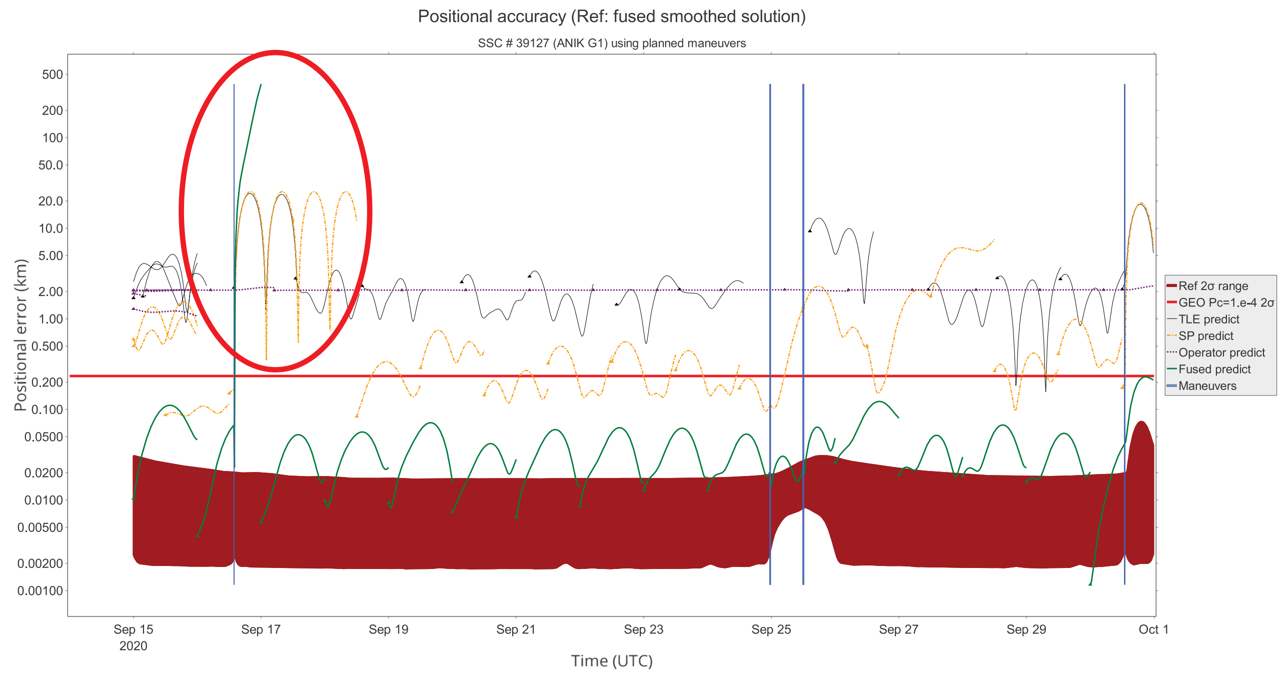

Fig. 9 Maneuver adversely impacting SP and Fusion solutions, as well as 2km operator bias (logarithmic scale).

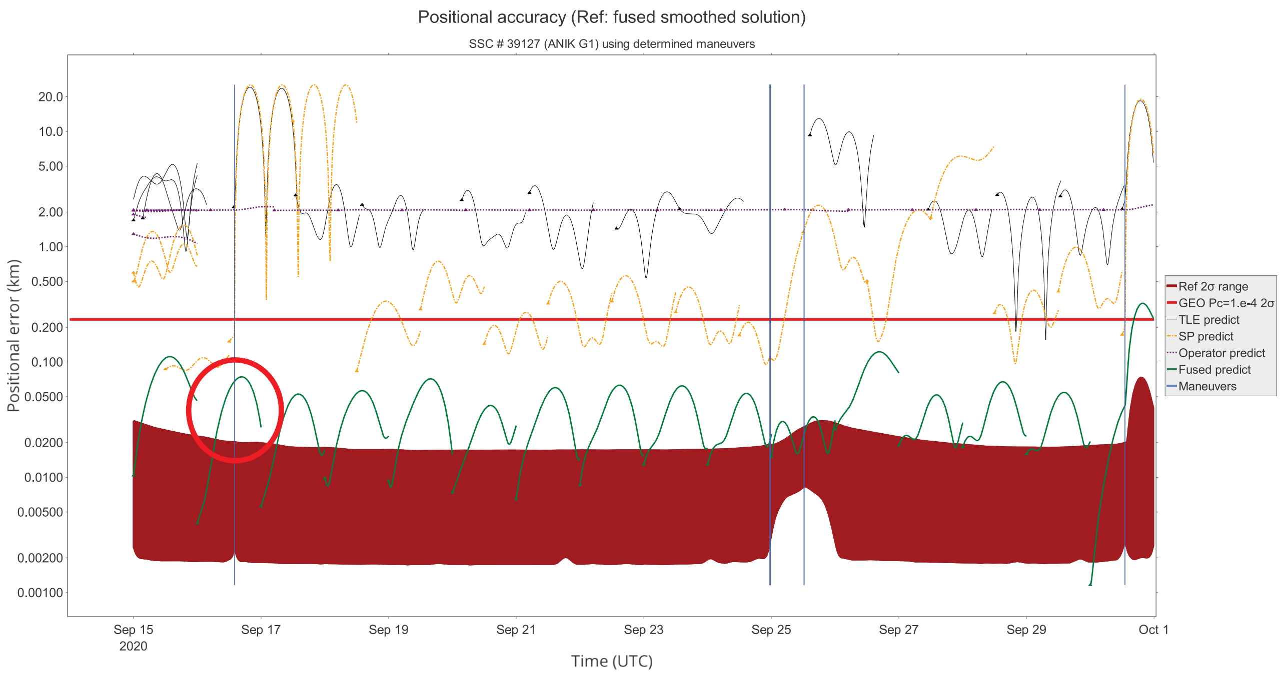

Fig. 10 Example of non-cooperative maneuver processing quickly recovering an accurate fused solution.

8 Benefit of data fusion in Launch and Early Orbit Phase

The estimated accuracy of the three Planet SkySat contained in the STCM demonstration generated interest in how well data fusion and close cooperation with the operator might help SSA and flight safety during the **Launch and Early Orbit Phase (LEOP)** for three Planet SkySat spacecraft. Accordingly, three SkySat spacecraft (C-17, C-18 and C-19) were analysed during the two weeks post-launch, which occurred on 18 August 2021.

Soon after launch, these spacecraft use low-thrust manoeuvring to raise their orbits from an orbit insertion altitude of 350 km up to their operational altitude at 440 km. Such low-thrust manoeuvring presents challenges for SSA systems, as they often have difficulty maintaining custody of the spacecraft. **Fig. 11** through **Fig. 13** provide the equivalents of **Fig. 8** for three SkySat spacecraft during the launch and early orbit phase.

Several things are apparent from these figures:

1) TLE (black line) and SP (orange line) data for the spacecraft are not (at least publicly) available until a week after launch (that occurred on 18 Aug 2020).
2) Once SP and TLE data become available, their error profiles are nearly identical to each other, likely driven by the unmodeled maneuvers that the spacecraft are conducting.
3) The operator's ephemerides (purple lines) are not made available until after TLEs and SP data have been released, per operator policy.
4) The overall lack of SkySat space data during LEOP could potentially impact safety of flight, SSA, and STCM assessments.

It can be seen from the red signature at the bottom of these figures that the GPS NavSol reference orbit is very accurate (on the order of 5 meters). Note the unavailability of the SP, TLE and owner/operator positional data for a week or more after launch.

Data fusion orbit determinations that incorporate Navigation Solution (NavSol) observational data typically provide very good accuracy, both at epoch and during the first twelve hours following epoch.

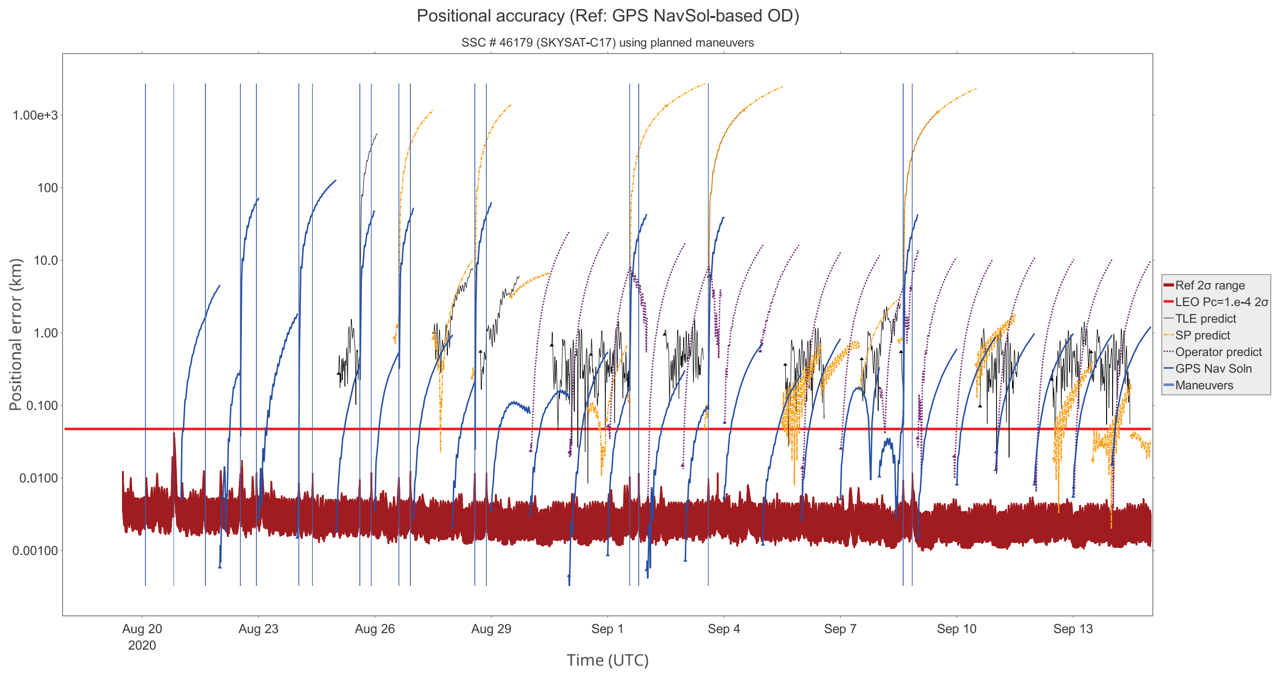

Fig. 11 LEOP accuracy of TLE, SP, operator and COMSPOC positional knowledge for SkySat C-17.

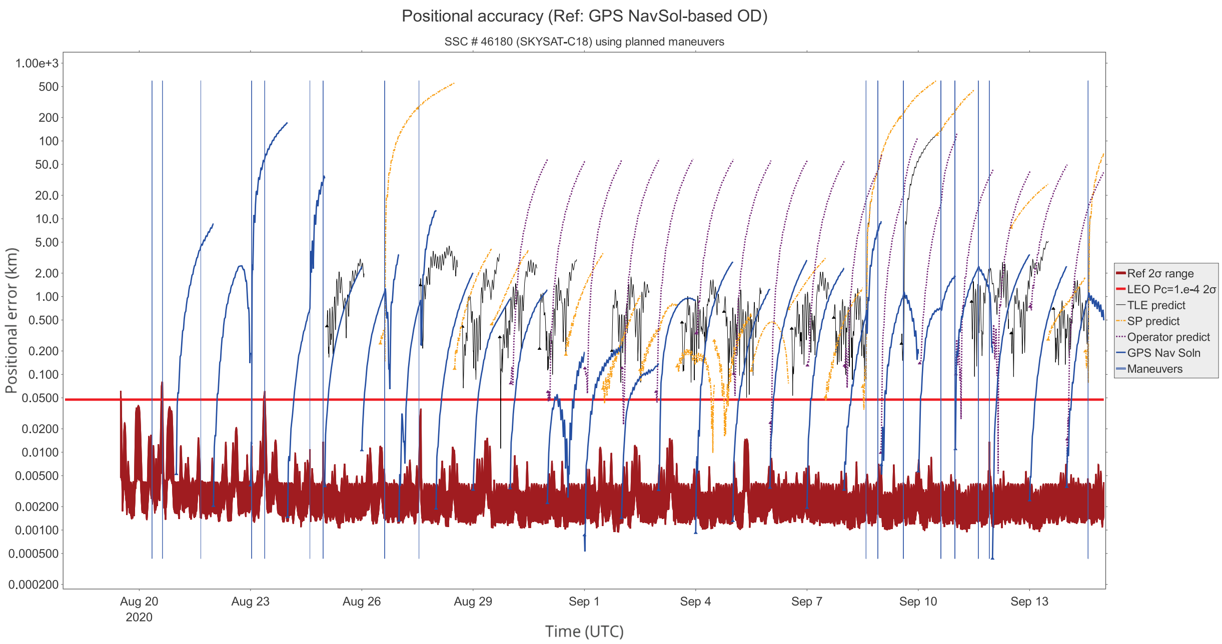

Fig. 12 LEOP accuracy of TLE, SP, operator and COMSPOC positional knowledge for SkySat C-18.

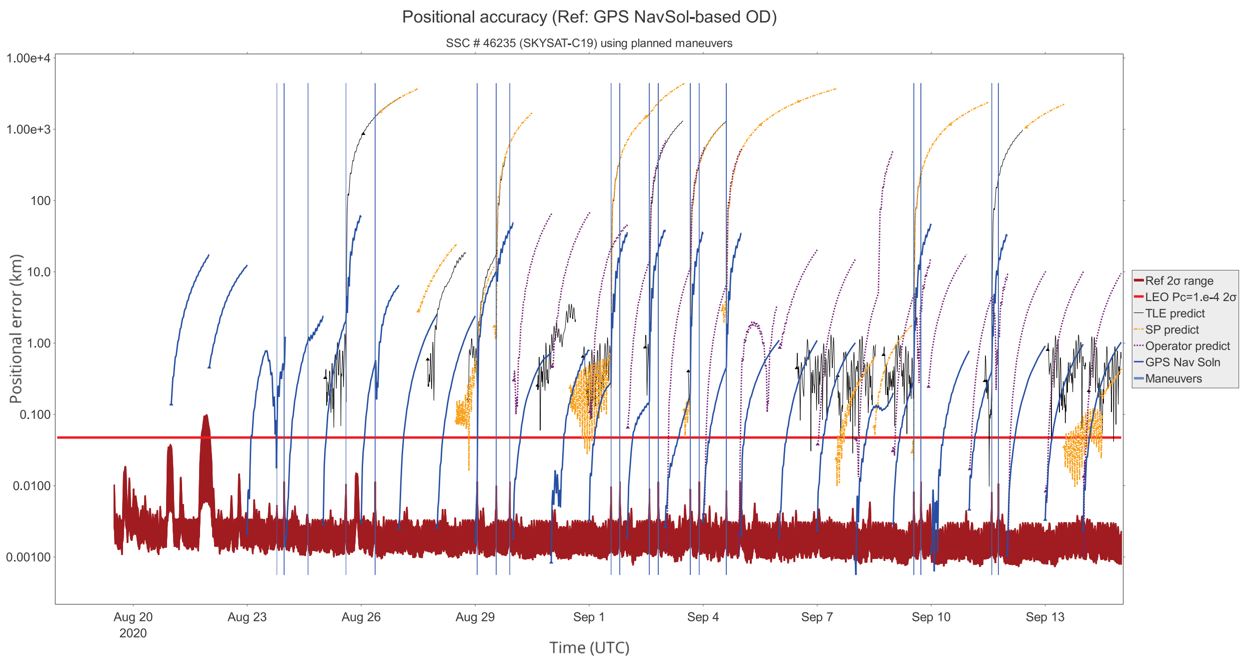

Fig. 13 LEOP accuracy of TLE, SP, operator and COMSPOC positional knowledge for SkySat C-19.

9 Statistical aggregation of SSA accuracy

When the above positional accuracy characterizations are aggregated across a statistically significant number of individual spacecraft, conclusions can be reached regarding the relevance, utility, and error profiles of the SSA products being used for these spacecraft. Relevant to this brief STCM data fusion demonstration, many more trials and data sets would need to be analysed to be conclusive.

But as a sample (and perhaps indicative) demonstration of the performance of SSA products, the error distribution can by aggregated as shown in **Fig. 14**. From this distribution, a percentiles-of-accuracy graph can be generated as shown in **Fig. 15**. This plot is one of the key products of the demonstration, characterizing the overall performance for these various SSA products for the LEO, MEO and GEO orbit regimes that our seventeen spacecraft occupy in this limited experiment.

The LEO statistical aggregation shown in **Fig. 15** corresponds to the 95th percentile accuracy, meaning that 95% of the accuracy samples exhibit better accuracy than the plot lines and the remaining 5% have worse accuracy.

As expected, the limited accuracy of the TLE's SGP semi-analytic theory (shown in the white line) does not fare as well as the other products at OD epoch, but an interesting result is that this accuracy does not appear to degrade as quickly as some other products in both the short- and long-term.

The blue line is the performance of orbit predictions based upon orbit determination of GPS-based NavSol observations, showing a very accurate solution even at the 95th percentile. The green line is the fused solution (in which we intentionally chose to exclude NavSol data). The orange trend depicts SP positional accuracy, the purple line represents owner/operator ephemerides.

In LEO, the NavSol solution improves upon legacy SSA positional accuracy by a factor of perhaps five in the first day, while the Fused solution still improves upon SP accuracy by roughly 10 to 50% (the divergent nature presumably due to the lack of incorporation of planned maneuvers in legacy SSA products). That said, even for these improved positional products, achieving the stringent sample accuracy requirement associated with a 1.e-4 Pc threshold is quite difficult, particularly at this high percentile value.

In GEO, comprehensive data fusion yielded a much greater accuracy improvement, with fused and NavSol accuracies ranging between ten and thirty times better in positional accuracy than legacy products at the 80th percentile.

The full set of accuracy percentiles characterizations is provided for the seventeen spacecraft in Appendix 3, and for the three LEOP SkySat spacecraft in Appendix 4. While we provide accuracies at the 50th percentile (typical or median performance), 80th and 95th percentiles, we assume that for an operational STCM system, one would need nearly all orbits (e.g., 95%) to be of acceptable accuracy, rather than using a typical (50th percentile) metric where half of the objects have worse accuracy than that percentile.

Fig. 57 - **Fig. 59** indicate that the fused solution accuracy is at least a ten-fold improvement over legacy SSA products, whereas **Fig. 63** - **Fig. 65** depict the ten to fifty percent fused LEO solution accuracy improvement at 95th percentile, and similar accuracies at typical (50th percentile) performance.

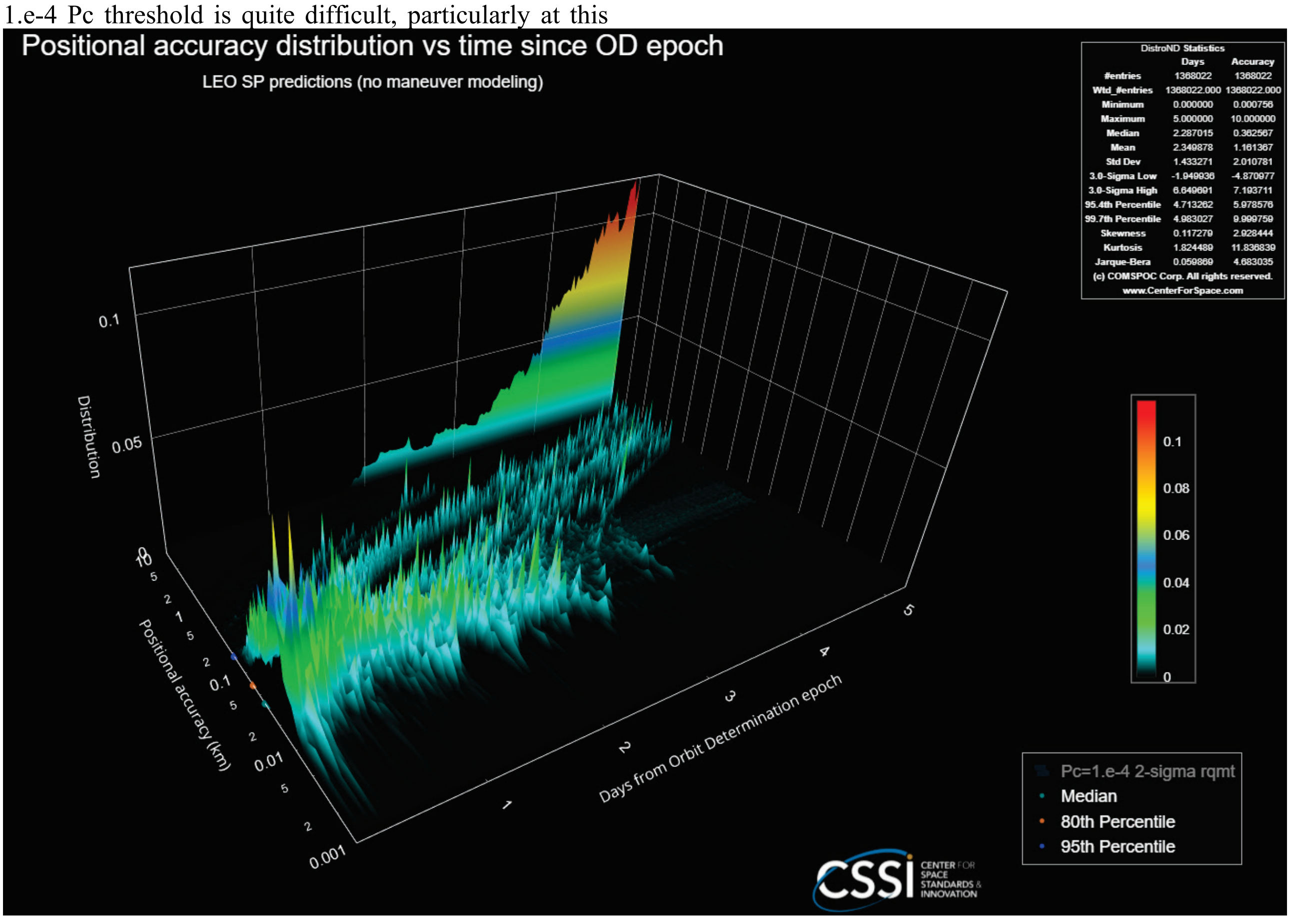

Fig. 14 NavSol accuracy distribution for 3 SkySat spacecraft, 18 Aug to 15 Sep 2020.

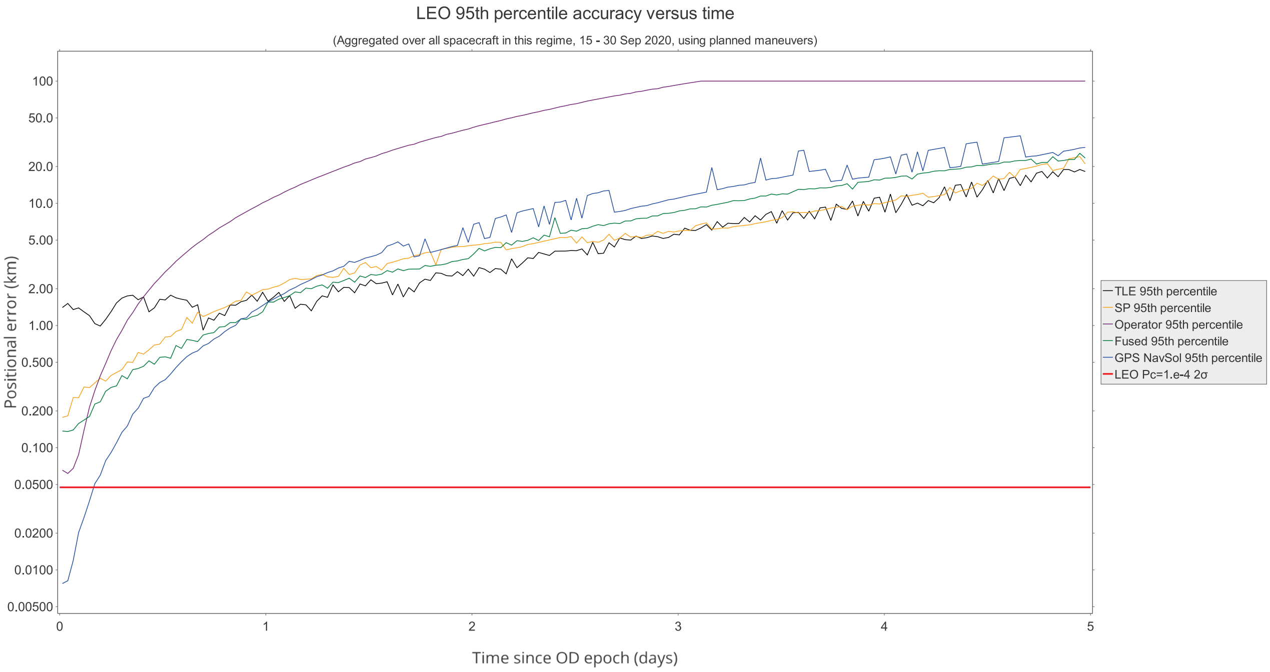

Fig. 15 95th percentile accuracy for portion of seventeen spacecraft in the LEO orbit regime.

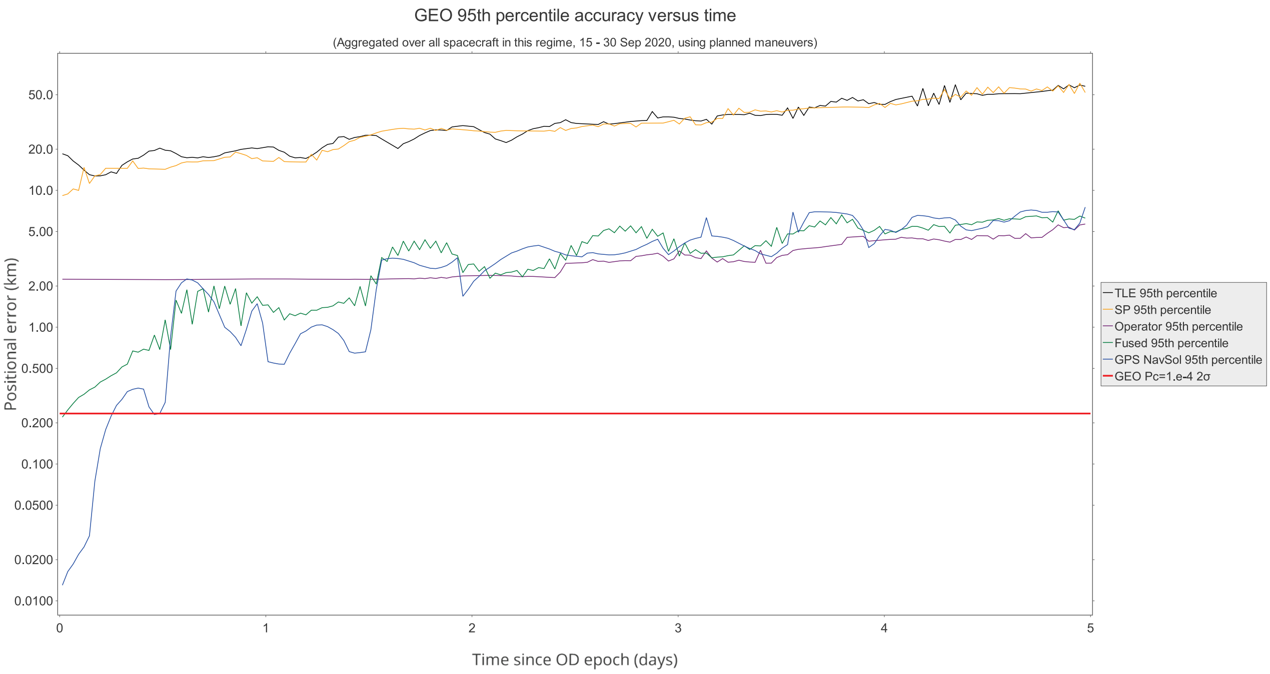

Fig. 16 95th percentile accuracy for portion of seventeen spacecraft in the GEO orbit regime.

10 Covariance realism tests

As presented above, accuracy assessments involve an estimated positional time history as compared to a reference orbit. The reference orbit is typically a smoothed ephemeris fit to all available observations after the fact. As such, it is often treated as the actual position of the object over the time of interest. But as shown above, even such smoothed reference orbits still have time-varying positional errors.

For this reason, efforts to gauge the "realism" of covariance (error) data must accommodate errors in both the estimated positional SSA product (e.g., the "fused" orbital position) as well as errors in the reference orbit.

To assess the variance between two orbital position estimates, we assume their uncertainties are zero-mean, Gaussian, and uncorrelated. Because the covariance matrices are uncorrelated, they are summed to form one, large, combined, covariance. The Mahalanobis distance between the mean positions is found from the combined positional covariance C and relative mean positions [x y z] through the equation.

$$d_{maha}{}^{2} = [x \quad y \quad z]\ C^{-1}\begin{bmatrix} x \\ y \\ z \end{bmatrix} \qquad (6)$$

Knowing the Mahalanobis distance, the value of sigma along the relative position vector is

$$\sigma = \sqrt{\frac{x^2+y^2+z^2}{d_{maha}{}^{2}}} \qquad (7)$$

10.1 Relationship between sigma span and probability density percentage

On method to examine covariance realism is to evaluate the percentage of time within a large ensemble of error trials that those errors lie within the estimated covariance.

The fraction of total, Gaussian, probability density spanning $-n\sigma$ to $+n\sigma$ is dependent on the dimensionality of the space. Gaussian PDFs in one, two and three dimensions are shown in ***Fig. 17***, ***Fig. 18***, and ***Fig. 19***.

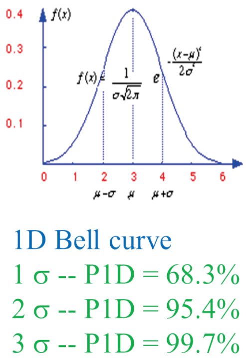

Fig. 17 One-dim. Gaussian.

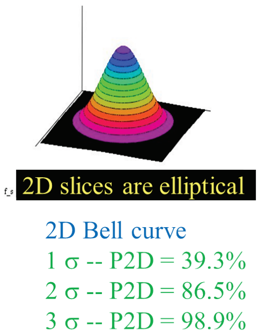

Fig. 18 Two-dim. Gaussian.

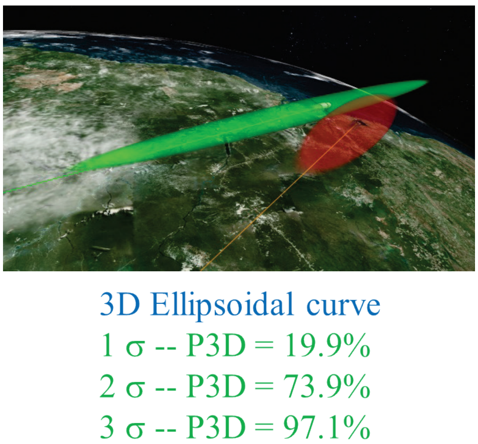

Fig. 19 Three-dim. Gaussian

The central message is that if a covariance matrix properly represents the ensemble of errors, a prescribed sigma level in one, two or three dimensions should in turn encompass the corresponding percentage of errors observed over a sufficiently large data set. Unfortunately, we do not have such a data set, but the methods can be applied to illustrate the use case.

To determine the percentage of a Gaussian error distribution encapsulated within a bounding number of sigma values ($\pm n\sigma$) along a single dimension, the equation is

$$P_{1D}(n) = \frac{1}{\sqrt{2\pi}}\int_{-n}^{n} e^{\left(\frac{x^2}{-2}\right)} dx\,. \qquad (8)$$

It should be noted that this equation is independent of the actual value of σ. Integration of the PDF along a line from -2σ to $+2\sigma$ would contain 95.4499736% of the total probability density ($P_{1D}(2) = 0.954499736$).

For two dimensions, the equation is

$$P_{2D}(n) = \frac{1}{2\pi}\int_{-n}^{n}\int_{-\sqrt{n^2-x^2}}^{\sqrt{n^2-x^2}} e^{\left(\frac{x^2+y^2}{-2}\right)} dydx \quad . \qquad (9)$$

A circle of radius 2σ would contain 86.4664716763% of the total probability density ($P_{2D}(2) = 0.864664716763$). The same applies to an elliptical shell of 2σ.

For three dimensions, the equation is

$$P_{3D}(n) = \frac{1}{\sqrt{8\pi^3}}\int_{-n}^{n}\int_{-\sqrt{n^2-x^2}}^{\sqrt{n^2-x^2}}\int_{-\sqrt{n^2-x^2-y^2}}^{\sqrt{n^2-x^2-y^2}} e^{\left(\frac{x^2+y^2+z^2}{-2}\right)} dzdydx \qquad (10)$$

The percentage of total probability density contained in a 2σ spherical or ellipsoidal shell is 73.8535870068% ($P_{3D}(2) = 0.738535870068$).

10.2 Using the Chi-Squared Metric

Others suggest using the Chi-Squared (χ^2) metric to the miss distance problem [4] and for examining covariance realism [5, 6], or more sophisticated Goodness of Fit (GOF) techniques [5] for assessing covariance realism. In this paper we assessed the percentile approach (presented above) to evaluate the scale factor (ideally 1.0) and the χ^2 metric (ideally 3.0 with standard deviation of 2.333 per [6]).

10.3 Sample covariance realism assessments

A sample result obtained by applying Equation (6) to one of the seventeen spacecraft is shown in ***Fig. 20***, exhibiting a scale factor of 1.1 and an χ^2 average and standard deviation of 3.4 and 2.6, respectively.

Achieving realistic error covariances requires accurate calibration, incorporation of force modelling errors, prior knowledge of maneuver uncertainties, and sufficient observational sampling (all of which were not practical during this short data fusion demonstration).

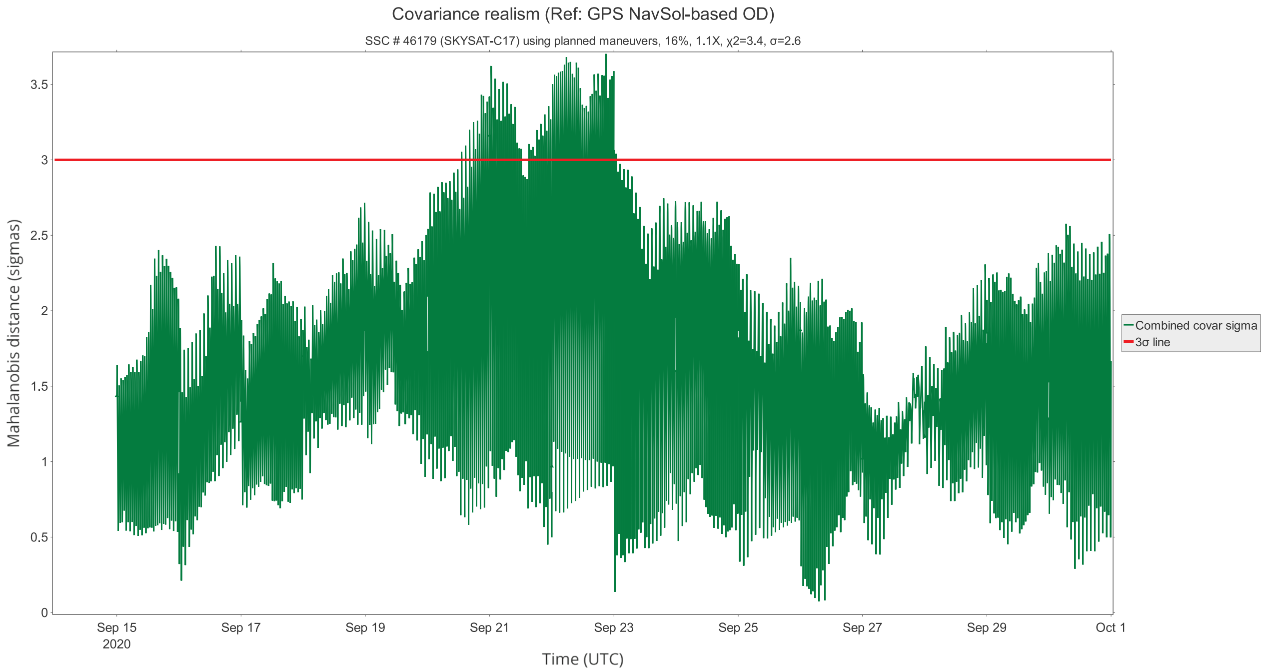

Fig. 20 Sample covariance realism plot using Mahalanobis distance metric

11 The role of industry and government in achieving effective space flight safety

The demanding accuracy requirements specified in Section 3 can only be achieved via close cooperation between the Satellite Operators and support from Governments and commercial SSA service providers.

11.1 Role of Industry

The Space Data Association (SDA) with its Space Data Centre (SDC) operated by AGI/COMSPOC is a very good example of cross-organizational data exchange between Satellite Operators. More than ten years ago, Intelsat, Inmarsat, SES, and Telesat pioneered this international approach to facilitate data collection, quality control, analysis, and reporting. The SDC provides services to 30 global operators of spacecraft spanning all orbital regimes, form factors and mission types. It performs safety-of-flight analyses for 683 spacecraft (411 spacecraft in LEO and MEO, and 272 spacecraft in GEO (51% of active).

The SDC enables significant SSA improvements thanks to the following two key elements:

1) The SDC framework incorporated data exchange technology to facilitate crowdsourcing and data exchange for safety of flight, in a Data Lake construct. During the last 10 years, the SDA and AGI/COMSPOC experts have demonstrated that effective SSA relies on using the best available data to manage close approaches. For active satellites, this implies that Satellite Operators shall exchange their maneuver plan information to generate reliable orbit propagation for SSA. This data exchange is mandatory for satellites using electric propulsion with frequent burns every day.

2) The SDC benefits from AGI/COMSPOC experts who closely monitor data quality by comparing information from diverse sources, revealing many discrepancies in SSA and operator space data products. GEO operators discovered for example that several of their satellites were operating a few hundredths of a degree away from their nominal longitude slot due to ranging biases.

Data exchange is essential but, to meet the accuracy requirements specified in Section 3, effective data fusion shall be implemented, requiring that more Operator observational data be shared. Indeed, Satellite Operators shall contribute additional raw measurements like:

- Standard tone ranging and azimuth/elevation measurements, transponder ranging.
- On-board GPS measurements.
- More advanced measurements like PaCoRa passive RF data relying on the time difference of arrival of the satellite payload signal at different ground stations [7].
- Optical or radar observations if available.

These raw measurements support effective data quality control and comprehensive data fusion to identify potential measurement biases and yield the best predictive information needed to assess collision risk and avoid confirmation bias. And finally, satellite dimensions and attitude data shall also be provided to support accurate probability of collision assessments.

11.2 Role of Governments

Ultimately, Space Situational Awareness should be the responsibility of international governmental organisations for the following reasons:

1) The cost of SSA efforts is already a huge burden for commercial operators. Today's SDC is not sufficient for effective STM (Space Traffic Management). The SDA looked to complement the CSpOC SP information and enable independent, accurate and reliable measurements or orbital information to implement data fusion but was not able to do so due to financial constraints.

2) STM is not geographically limited; any accidents affect global space commons.

3) STM is vital for all operators in space, including for national and international security efforts.

4) Most SSA systems rely on either the 18SPCS catalogue or the CSpOC/18SPCS warning system. To meet the accuracy requirements specified in Section 3 via data fusion, these systems need to be complemented by systems capable of tracking objects of all sizes, and by maintaining a reliable and independent catalogue of objects. These systems, either ground-based (radar, ground telescope) or space-based (constellation of satellites), are very expensive to deploy and operate.

5) Current systems typically track objects from 10 cm (LEO) to 1 m (GEO). However, ESA predicts that there are currently 900,000 objects in space between 1cm to 10cm in size and another 128 million objects between 1mm to 1cm. Even debris this small can cause horrendous damage to equipment, putting whole satellite operations at risk. Additionally, collisions between one or more large space objects have the potential to set off a chain reaction of secondary, tertiary etc. follow-on conjunctions. To this end, new technological innovations in tracking technology should be considered and will require massive investments in tracking systems and catalogue maintenance.

In addition to the services provided by the 18SPCS and SDA, there are several government-run initiatives that are good steps in the right direction. This includes European Space Surveillance and Tracking (EUSST), established by the European parliament in 2014 to ensure the long-term availability of the European space environment. In the US, the Department of Commerce has been designated as the lead civilian agency for providing basic SSA data and STM services to commercial space operators.).

12 Discussion and conclusions

For this limited set of 17 spacecraft participating in this STCM demonstration, we have shown the operational capability to fuse data from a wide variety of disparate sensors, sensor types, sensor networks, government and commercial SSA centers, and spacecraft observations, maneuver plans and ephemerides from spacecraft operators. This is not a competition, but rather a demonstration that hints at the potential for us to greatly improve accuracy, and as a result safety of flight, by comprehensive data sharing and fusion at the raw observational level.

The key elements of the demonstration were the comprehensive data fusion capability, advanced quality control and comparative SSA analytics, government SSA observations, and spacecraft operator contributions of spacecraft ephemerides, maneuver plans, and especially raw observation data. This demonstration highlighted the fact that predictive positional products that fail to incorporate planned maneuvers can be substantially degraded.

Operators and governments are typically able to choose their own conjunction metrics and associated thresholds. Irrespective of the chosen metric and threshold, each maps in some fashion to requirements on the accuracy of the underlying SSA framework. In the case of a collision probability threshold of one in ten thousand, results of this demonstration appear to indicate that without the sort of comprehensive data fusion demonstrated here, we are unable to meet accuracy requirements.

While this analysis of a relatively small but representative set of seventeen maneuvering spacecraft provides some insight into the achievable SSA accuracy for spacecraft, we recommend that this same type of assessment be performed for space debris and derelict spacecraft. Achieving accurate solutions for such debris can present challenges, to include the perturbations for High-Area-to-Mass-Ratio (HAMR) objects, the difficulties associated with tracking small debris fragments, and the tumbling nature of debris fragments (leading to drag, solar radiation pressure, and collision probability estimation challenges).

13 Recommendations

This has only been a limited experiment involving seventeen maneuvering spacecraft. Given the ever-increasing space debris population trends seen in **Fig. 21**, we recommend that priority be placed on extending this experiment to a broader and more comprehensive mix of spacecraft, orbital regimes, and added space debris, to generate more robust sampling and derived statistics and further explore accuracy and covariance realism characteristics as they relate to the STCM problem set.

14 Acknowledgements

We are grateful to all participants and contributors that made this STCM demonstration possible, including the U.S. government (Office of Space Commerce and U.S. Space Command), U.S. government and commercial spacecraft operators (Iridium, NOAA, Planet, SES, and Telesat), commercial SSA service providers (Kratos, Raytheon, Rincon, Thoth, and COMSPOC), the Space Data Association for their support and participation, and the University of Texas for their guidance, insights, and encouragement.

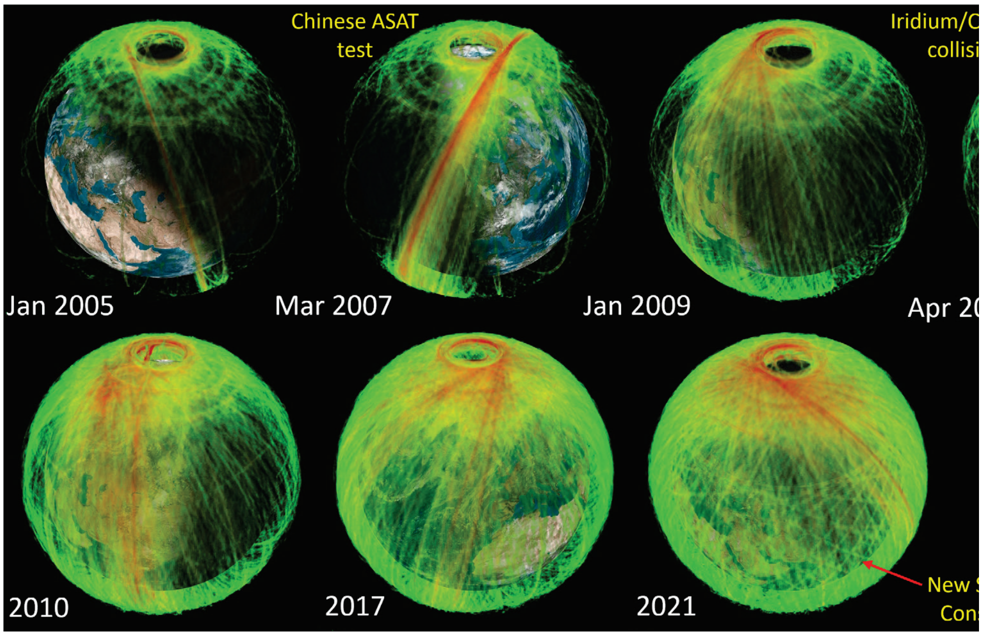

Fig. 21 Sixteen-year evolution of publicly tracked space debris now reflects new Large Constellations.

15 References

[1] Alfano, S., "Determining A Probability-Based Distance Threshold for Conjunction Screening," *AIAA Journal of Spacecraft and Rockets*, Vol. 50, No. 3, May-June 2013, pp. 686-690.

[2] Doerfler, R., "What is a nomogram?" http://www.myreckonings.com/modernnomograms/ [retrieved 8 February 2018].

[3] Fundamentals of Astrodynamics and Applications, 4th Edition, ISBN 978-1881883180, David A. Vallado and Wayne D. McClain, Published by Microcosm Press, 2013.

[4] Chan, K., "Miss Distance – Generalized Variance Non-Central Chi Distribution," AAS 11-175, 21st AAS/AIAA Space Flight Mechanics Meeting, New Orleans, Louisiana, 13-17 February 2011.

[5] Hejduk, M.D., et al, "Trajectory Error and Covariance Realism for Launch COLA Operations," AAS 13-355, AAS/AIAA Space Flight Mechanics Meeting, 10-14 February 2013.

[6] Tyler Lilly-Salkowski, "Filter Tuning Using the Chi-Squared Statistic," NASA-GSFC presentation, https://ntrs.nasa.gov/api/citations/20170005191/downloads/20170005191.pdf [retrieved 16 April 2021].

[7] Rodriguez, L., Krier, G., Thill, M. & de Vicente, J. (2014). Passive Ranging for Geostationary Satellites: On a Novel System and Operational Benefits. SpaceOps 2014 Conference. *American Institute of Aeronautics and Astronautics, AIAA-2014-1857.*

Appendix 1. Positional accuracy using planned maneuvers

The following seventeen figures provide estimated accuracy of the various SSA positional products using a logarithmic accuracy scale (y-axis). In each plot, the title indicates what the source of the reference orbit was, and the "Ref 2σ range" (red-filled area typically at the bottom of the plot) indicates the resultant estimated accuracy of the reference orbit. While the logarithmic scale allows all data to be clearly shown on a single plot (the estimated accuracy of the reference orbit is of particular interest), the log scale tends to deemphasize large positional errors while exacerbating small ones.

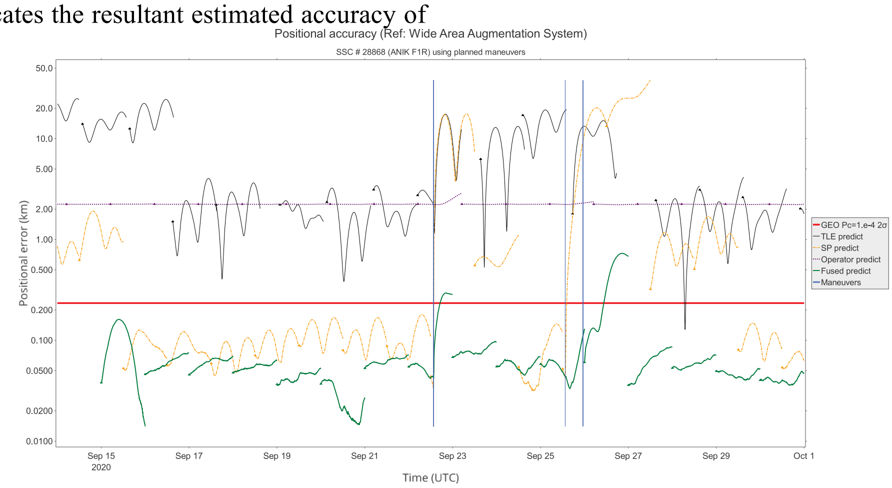

Fig. 22 GEO: ANIK F1R accuracy, planned maneuvers.

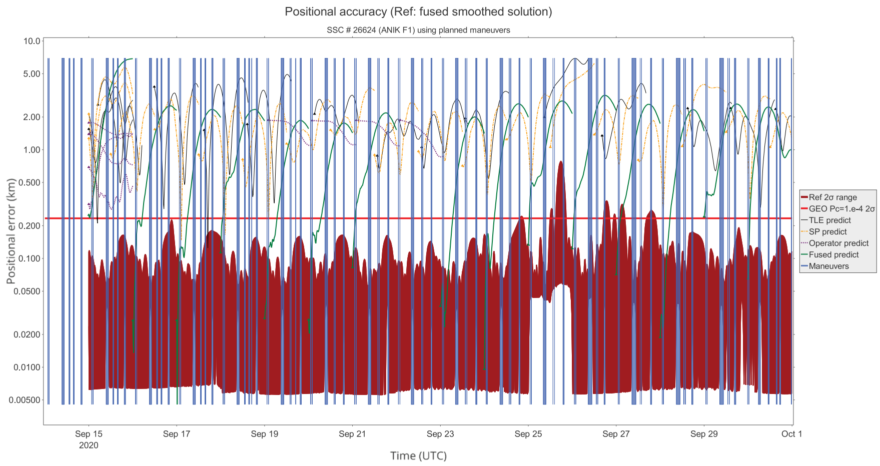

Fig. 23 GEO: ANIK F1 accuracy, planned maneuvers.

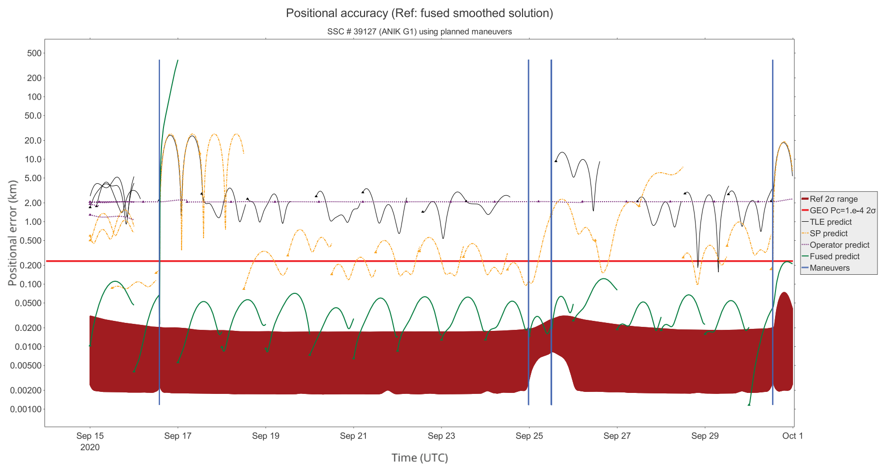

Fig. 24 GEO: ANIK G1 accuracy, planned maneuvers.

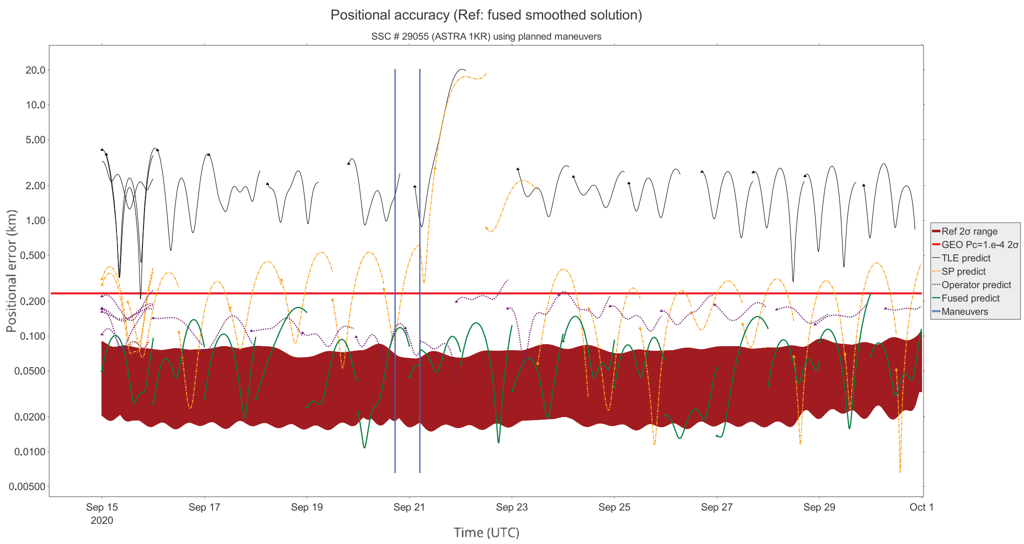

Fig. 25 GEO: ASTRA 1KR accuracy, planned maneuvers.

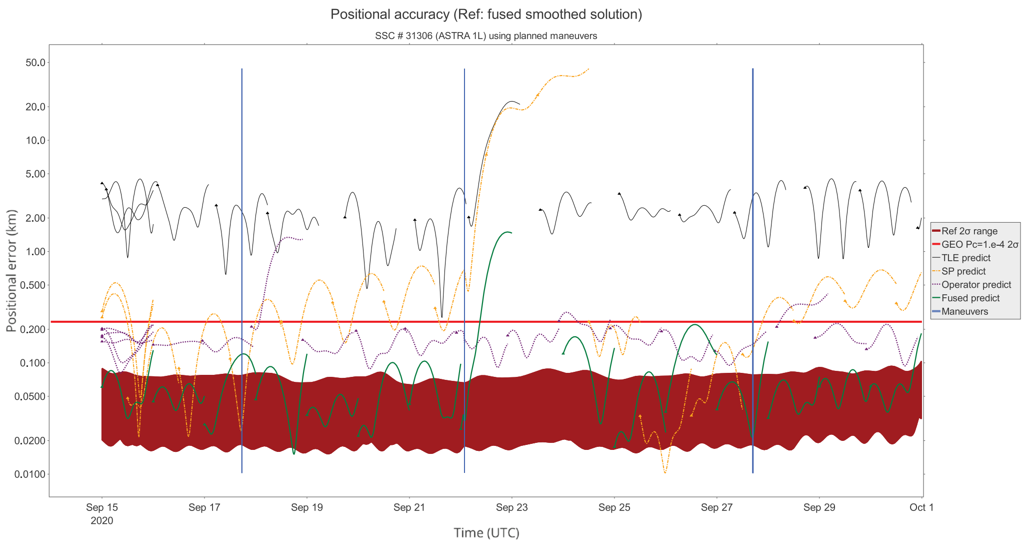

Fig. 26 GEO: ASTRA 1L accuracy, planned maneuvers.

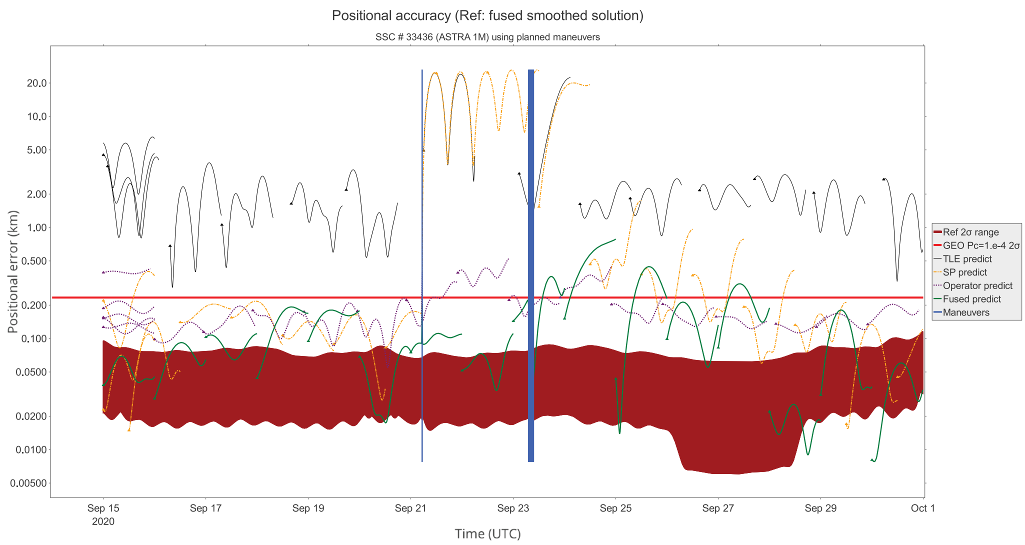

Fig. 27 GEO: ASTRA 1M accuracy, planned maneuvers.

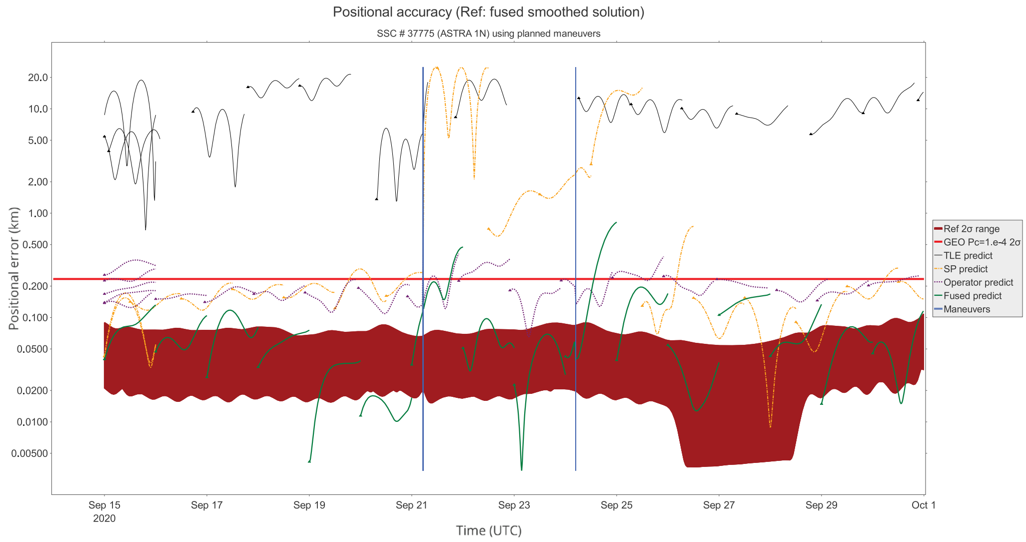

Fig. 28 GEO: ASTRA 1N accuracy, planned maneuvers.

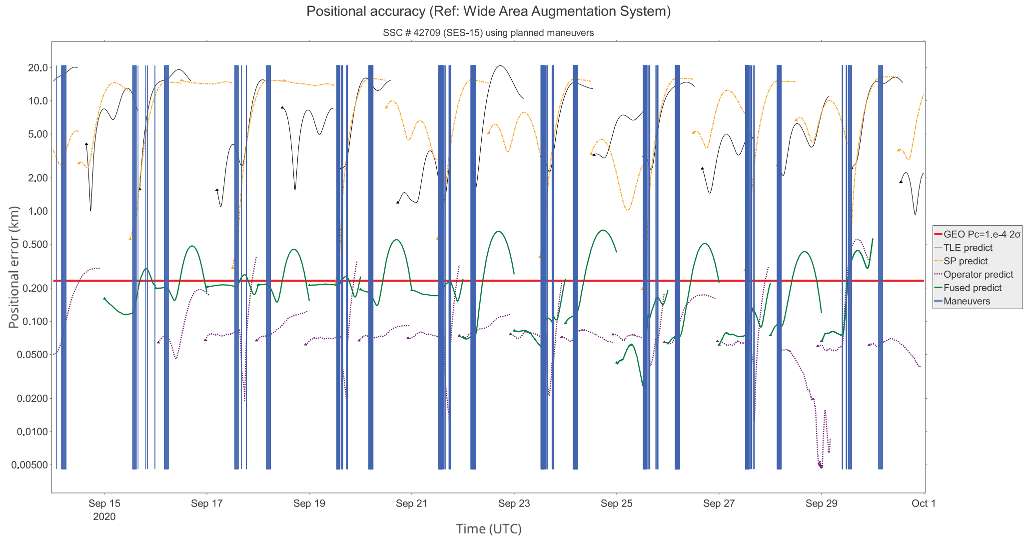

Fig. 29 GEO: SES-15 accuracy, planned maneuvers.

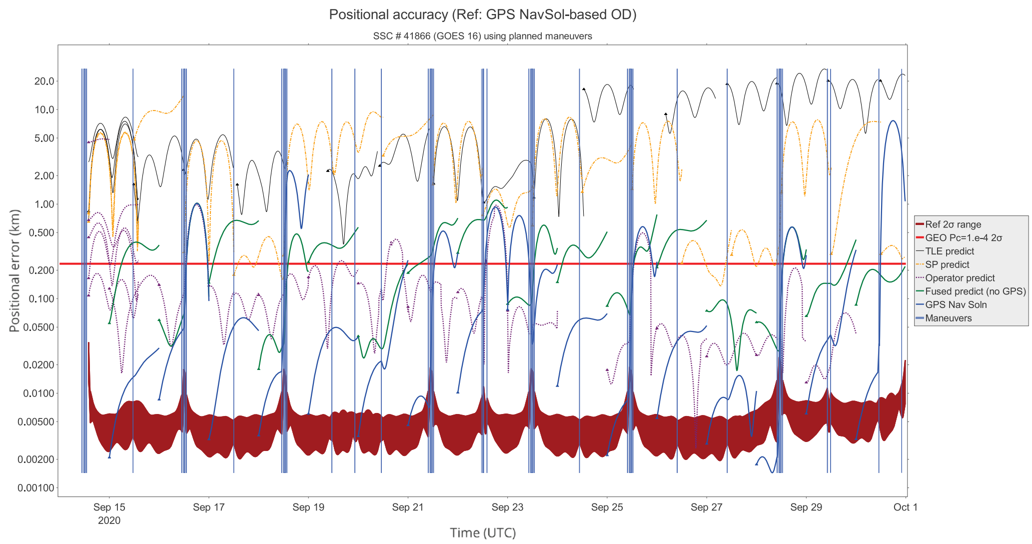

Fig. 30 GEO: GOES 16 accuracy, planned maneuvers.

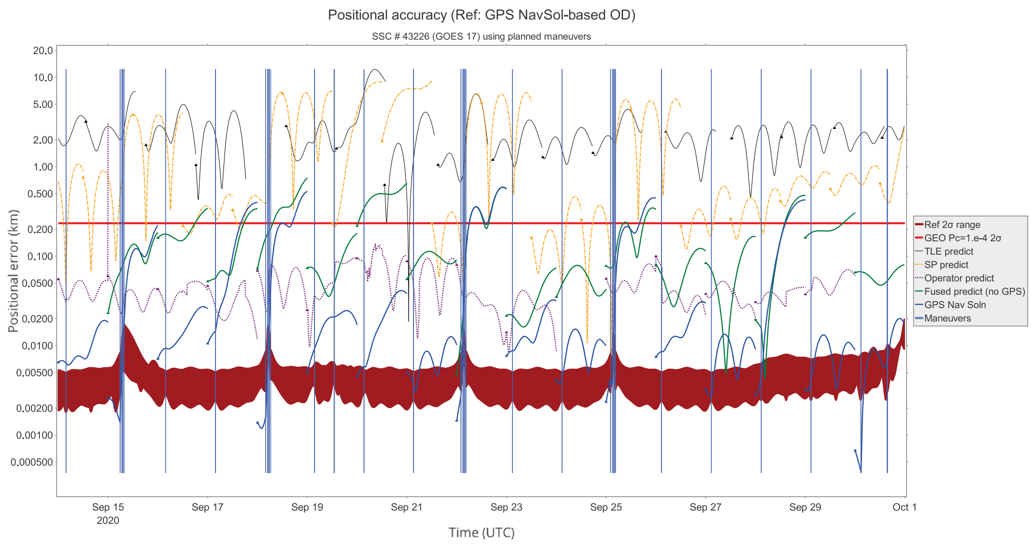

Fig. 31 GEO: GOES 17 accuracy, planned maneuvers.

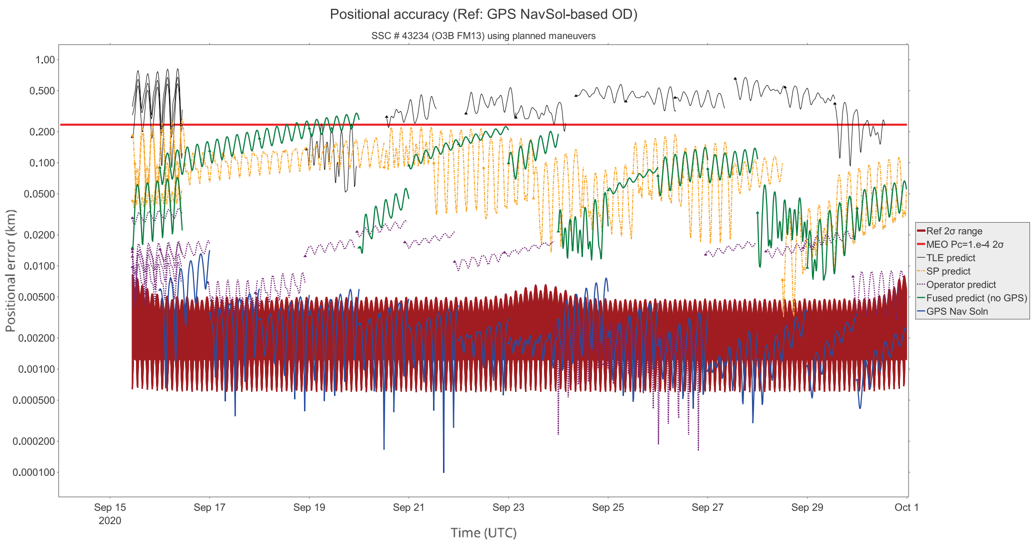

Fig. 32 MEO: O3B FM13 accuracy, planned maneuvers.

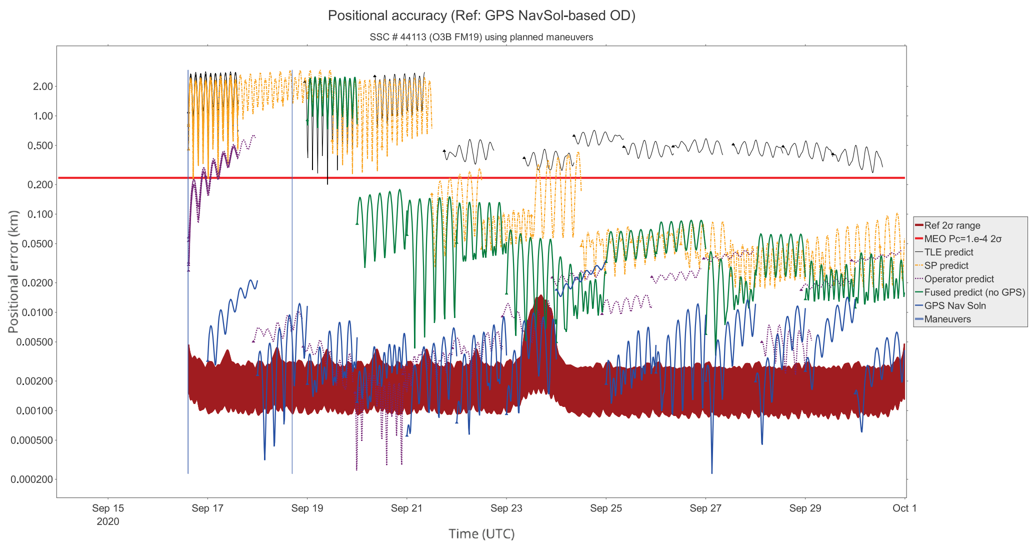

Fig. 33 MEO: O3B FM19 accuracy, planned maneuvers.

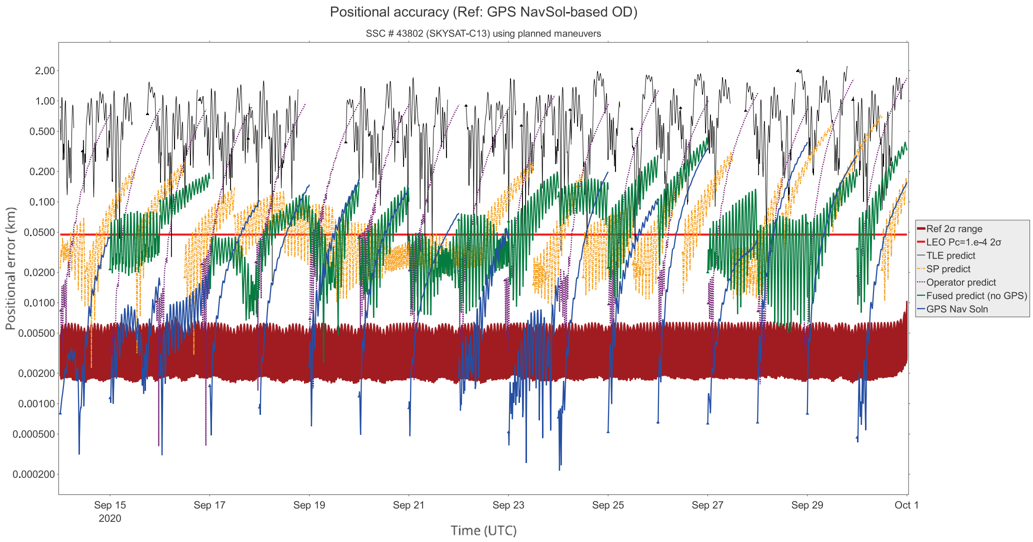

Fig. 34 LEO: Planet SkySat C-13 accuracy, planned maneuvers.

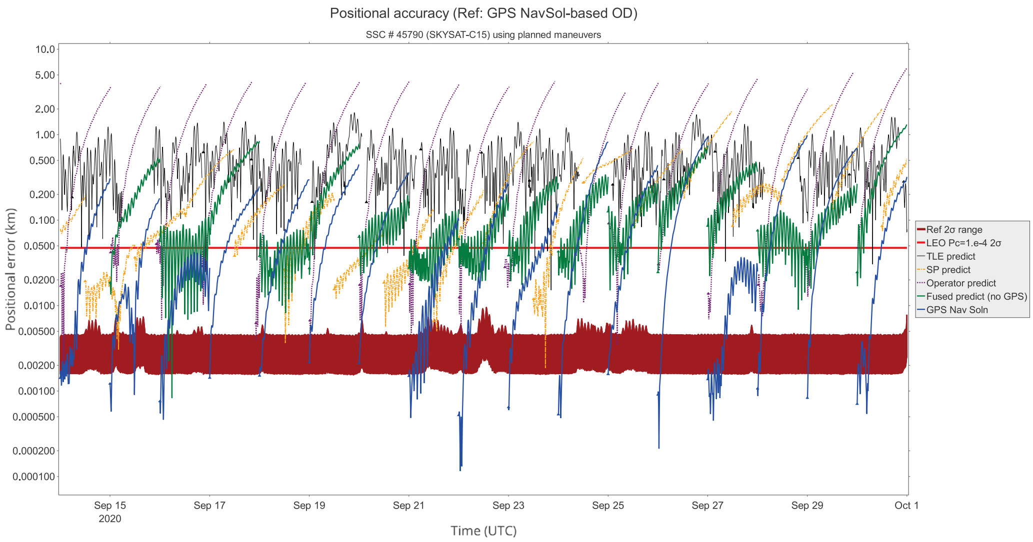

Fig. 35 LEO: Planet SkySat C-15 accuracy, planned maneuvers.

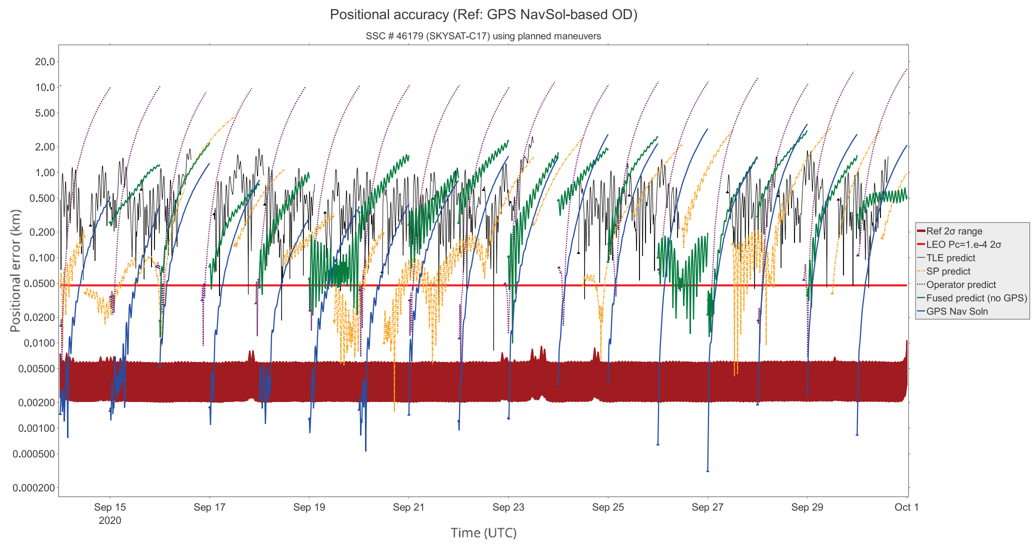

Fig. 36 LEO: Planet SkySat C-17 accuracy, planned maneuvers.

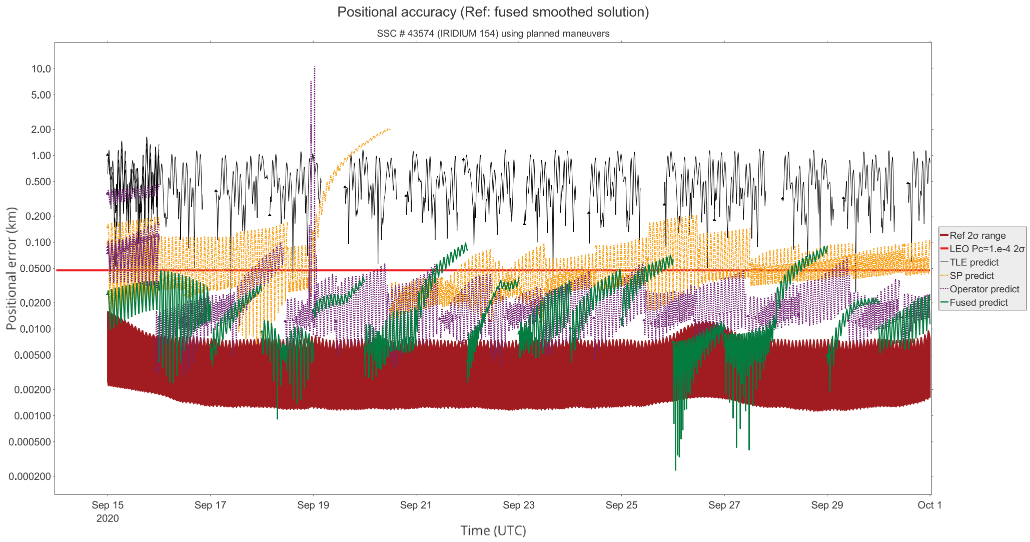

Fig. 37 LEO: Iridium 154 accuracy, planned maneuvers.

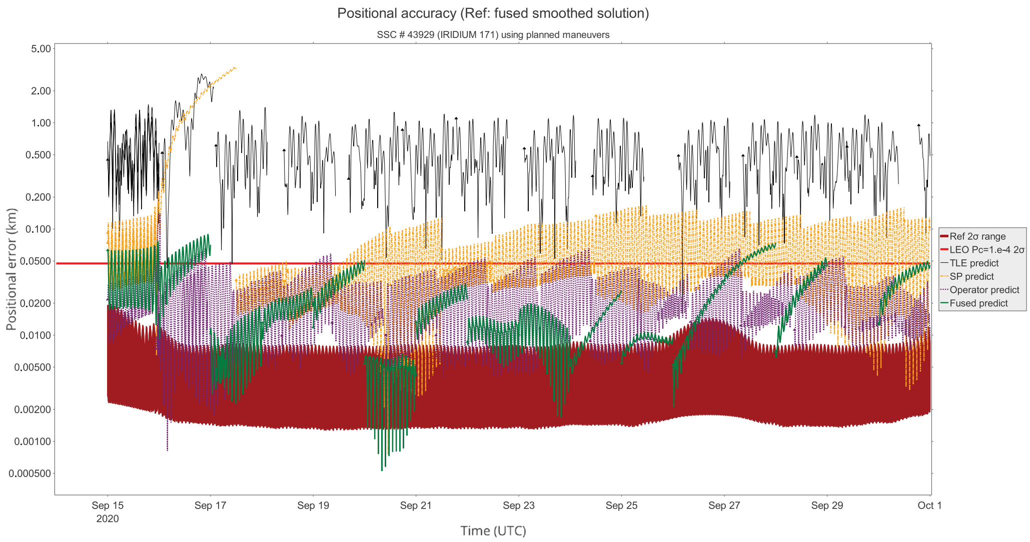

Fig. 38 LEO: Iridium 171 accuracy, planned maneuvers.

Appendix 2. Positional accuracy with determined maneuvers

Typically, the COMSPOC data fusion capability processed the observations and maintain an accurate solution with minimal operator intervention. But in cases where operator maneuver plans appeared to contradict what occurred, or the operator knew of the existence of a maneuver without knowing the exact maneuver time, direction and/or magnitude, the COMSPOC system non-cooperatively detected, characterized, incorporated and refined the maneuver. This section illustrates both achievable accuracy and the capability to maintain custody in the presence of unknown maneuvers.

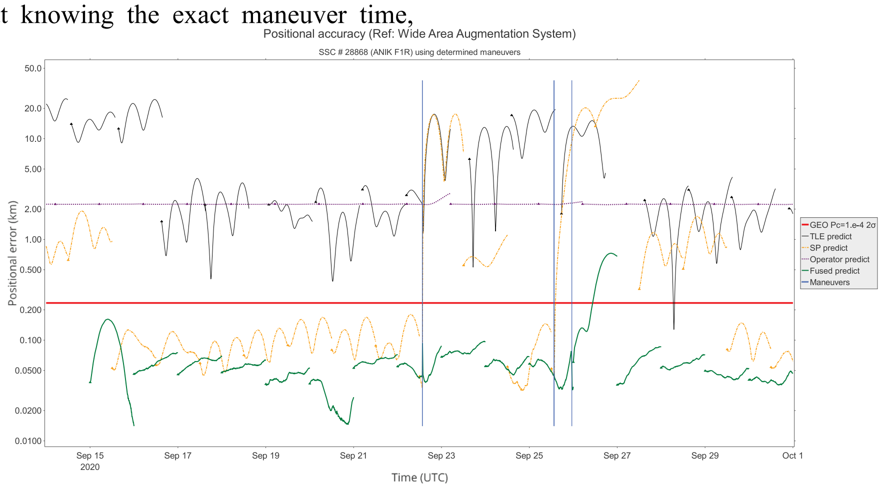

Fig. 39 GEO: ANIK F1R accuracy, determined maneuvers.

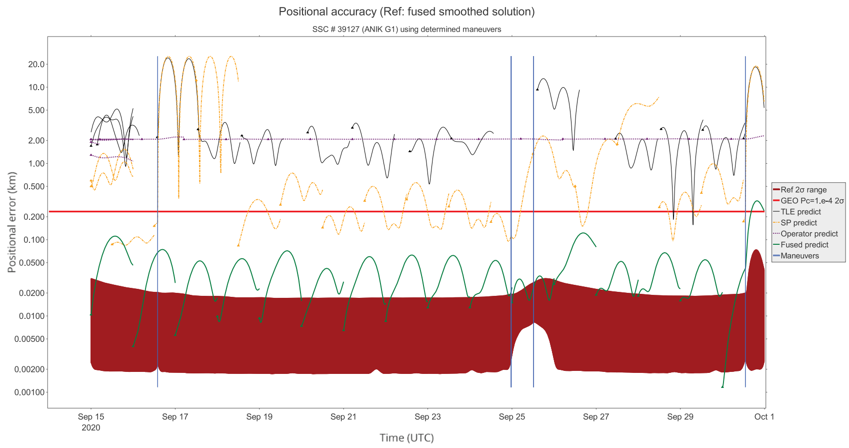

Fig. 40 GEO: ANIK G1 accuracy, determined maneuvers.

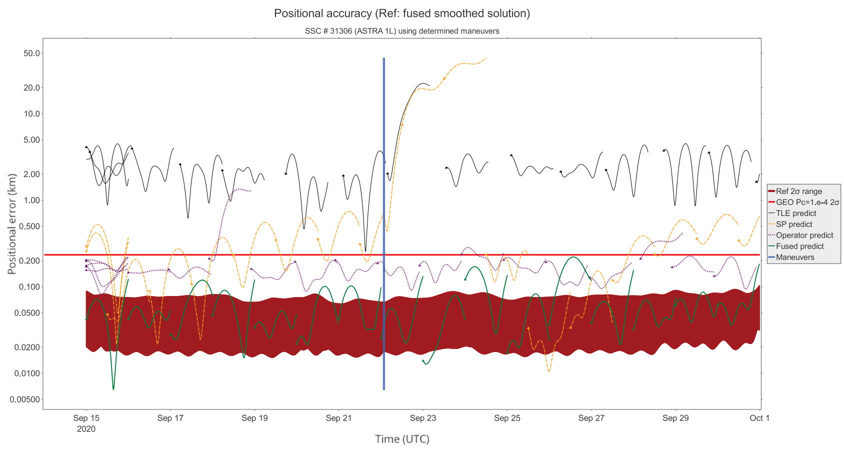

Fig. 41 GEO: ASTRA 1L accuracy, determined maneuvers.

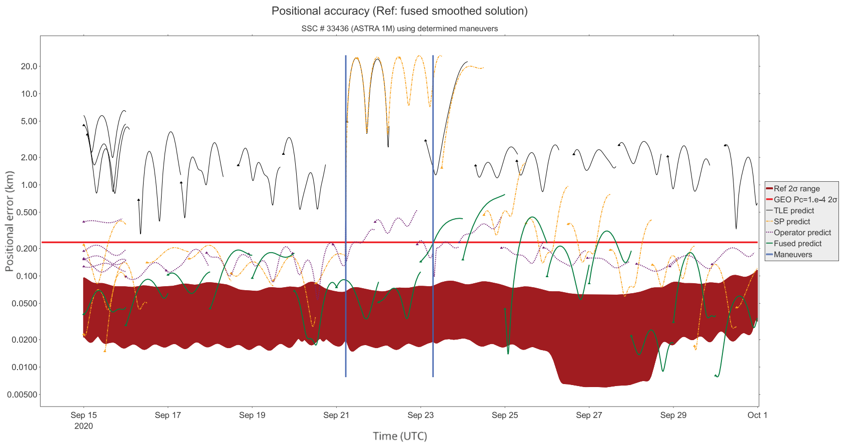

Fig. 42 GEO: ASTRA 1M accuracy, determined maneuvers.

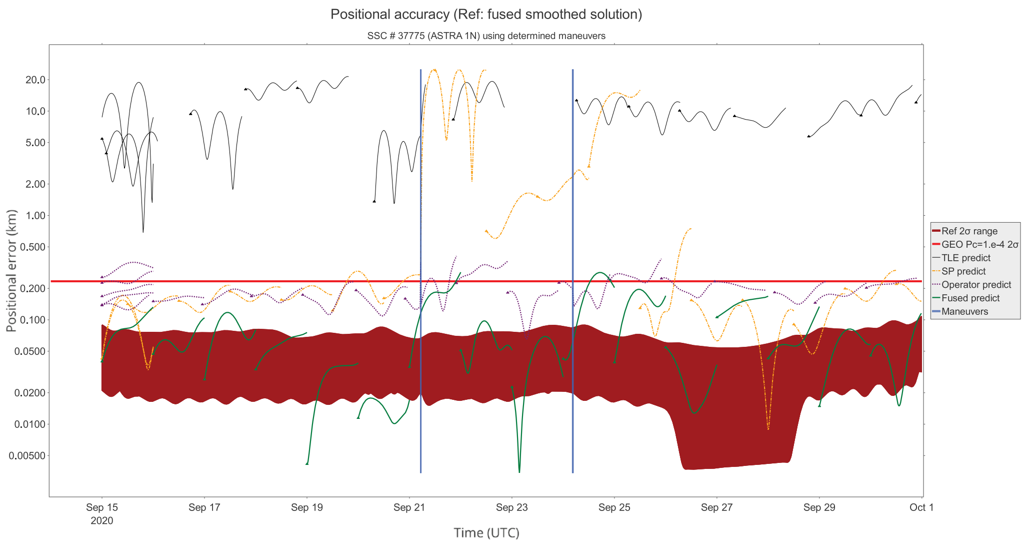

Fig. 43 GEO: ASTRA 1N accuracy, determined maneuvers.

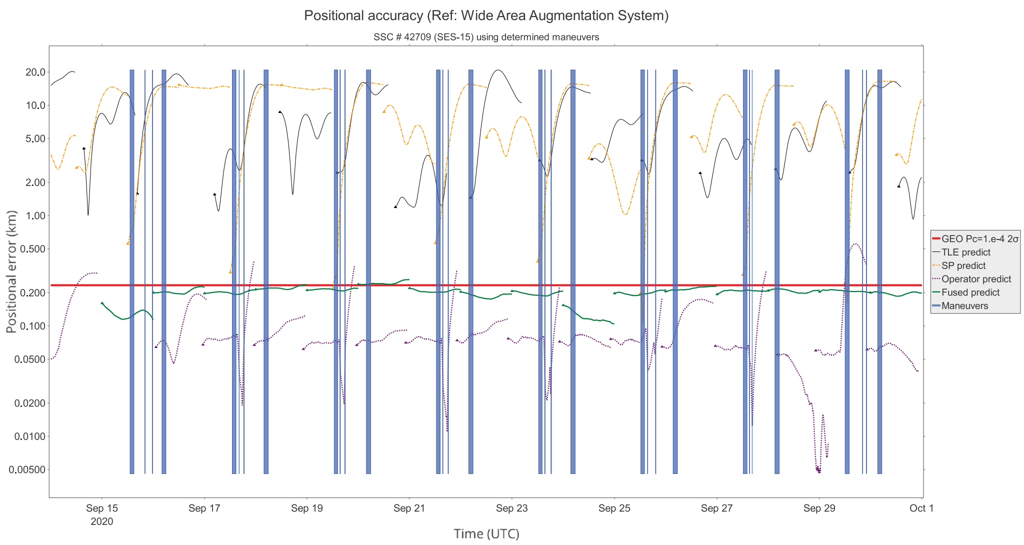

Fig. 44 GEO: SES-15 accuracy, determined maneuvers.

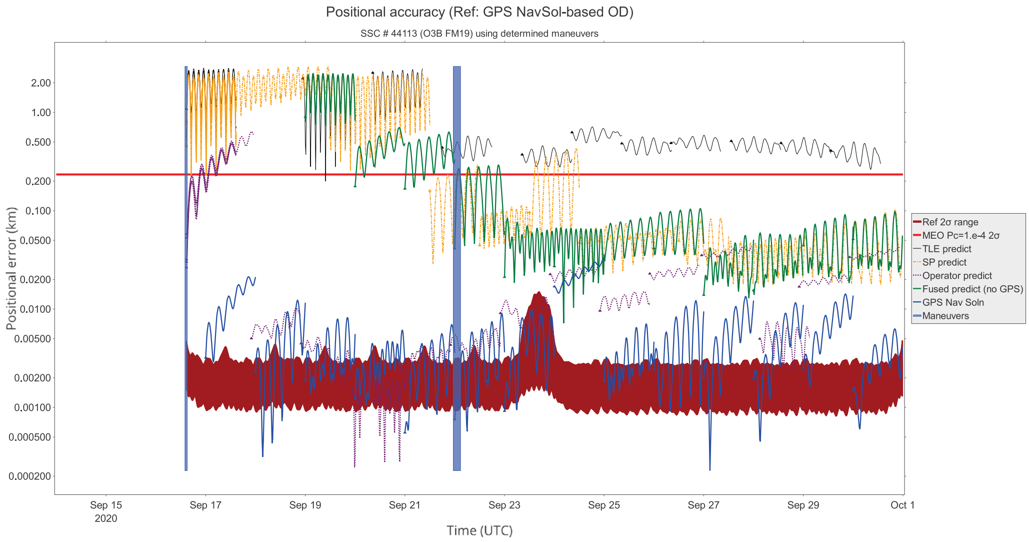

Fig. 45 LEO: O3B FM19 accuracy, determined maneuvers.

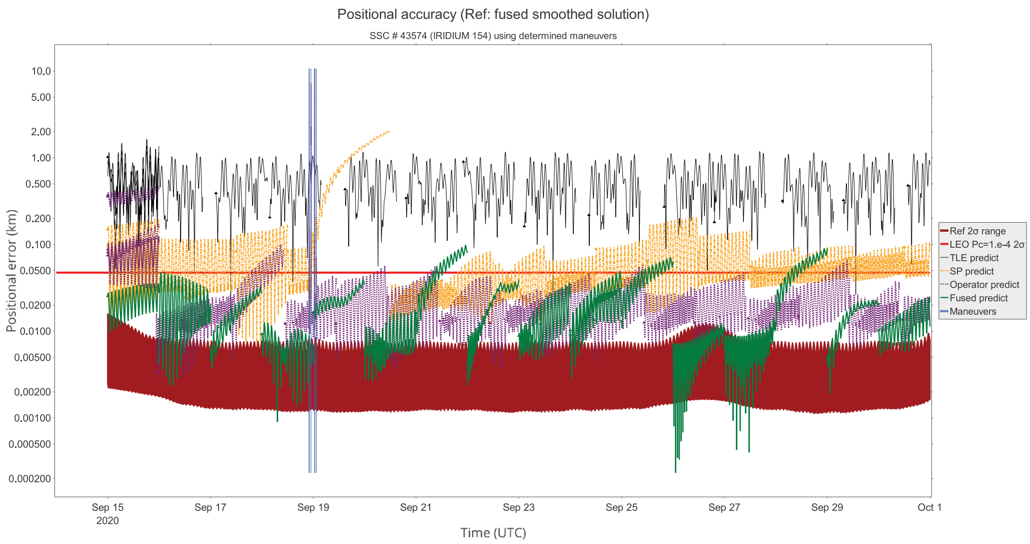

Fig. 46 LEO: Iridium 154 accuracy, determined maneuvers.

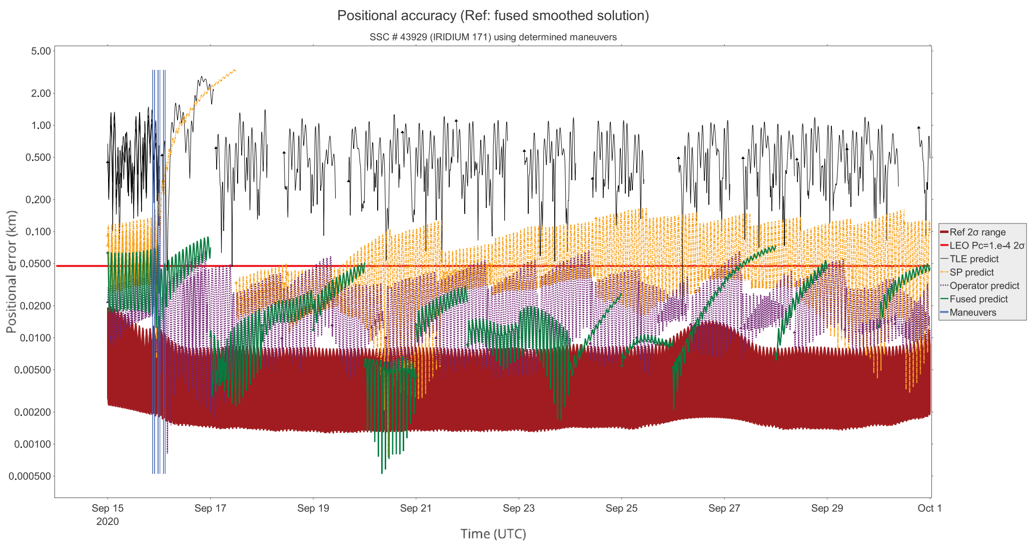

Fig. 47 LEO: Iridium 171 accuracy, determined maneuvers.

Appendix 3. STCM Demonstration accuracy statistics

The accuracies observed for this small set of seventeen spacecraft form a dataset that can be statistically analysed for each of the three orbit regimes (LEO, MEO and GEO) participating in this short demonstration. As discussed in the text, **this is a classically under-sampled data set**, and we must remember that such results are not conclusive. Ideally, this STCM demonstration should be conducted on a much larger data set over a longer period. Nevertheless, these results are likely indicative of the relative errors, gaps and SSA degradations and (conversely) benefits of the various SSA data products.

A3.1. Linear-scale accuracy stats

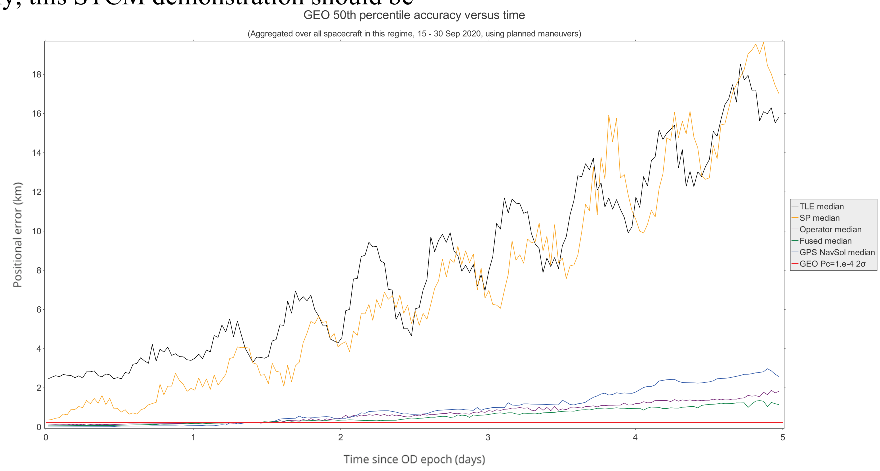

Fig. 48 GEO: 50th percentile positional accuracy versus sample accuracy requirement.

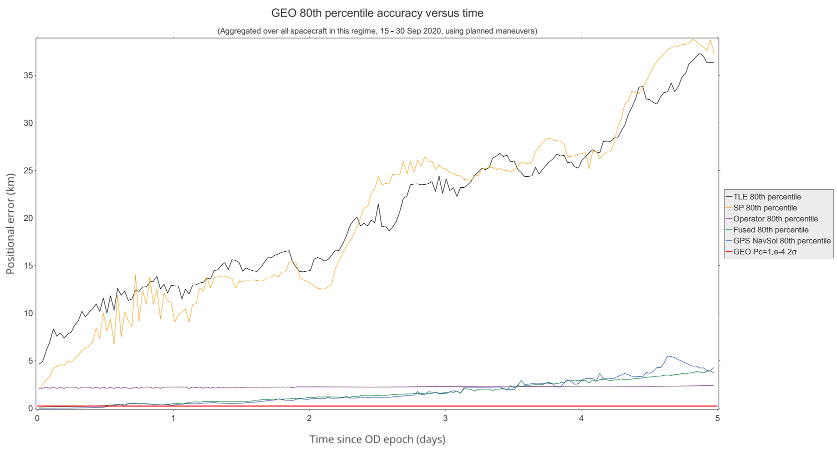

Fig. 49 GEO: 80th percentile positional accuracy versus sample accuracy requirement.

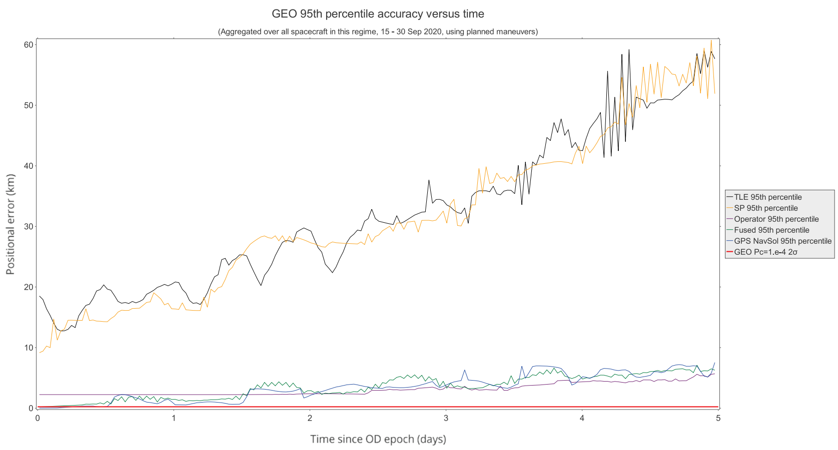

Fig. 50 GEO: 95th percentile positional accuracy versus sample accuracy requirement.

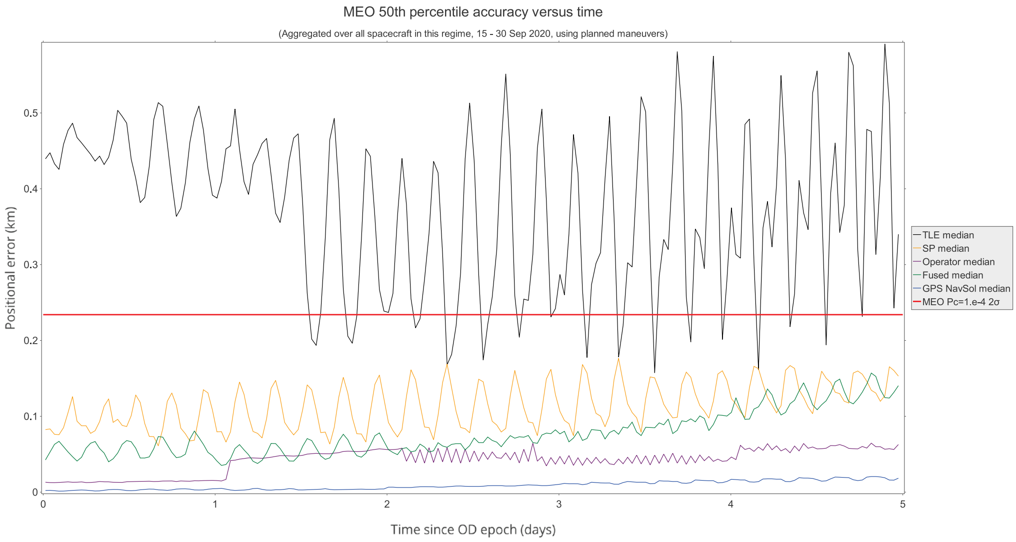

Fig. 51 MEO: 50th percentile positional accuracy versus sample accuracy requirement.

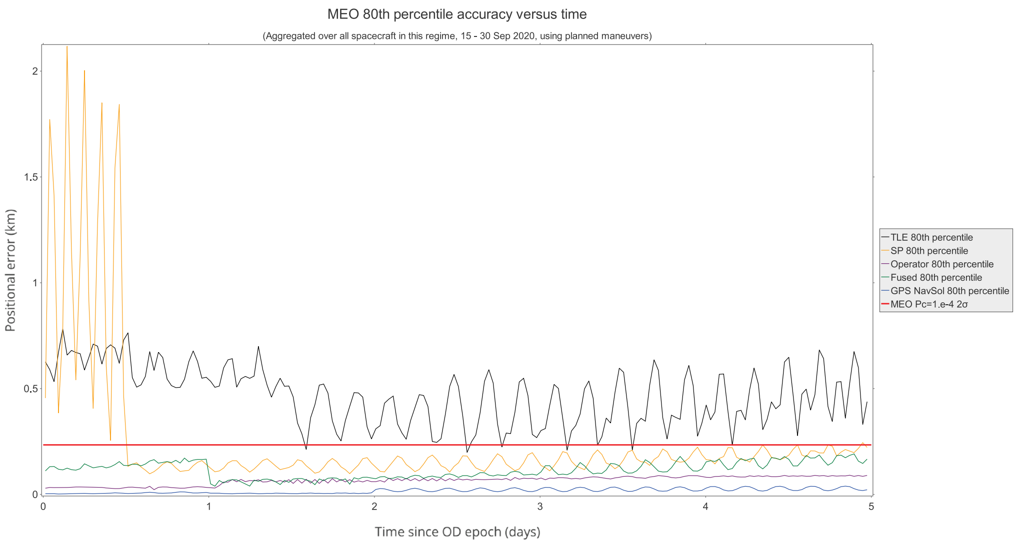

Fig. 52 MEO: 80th percentile positional accuracy versus sample accuracy requirement.

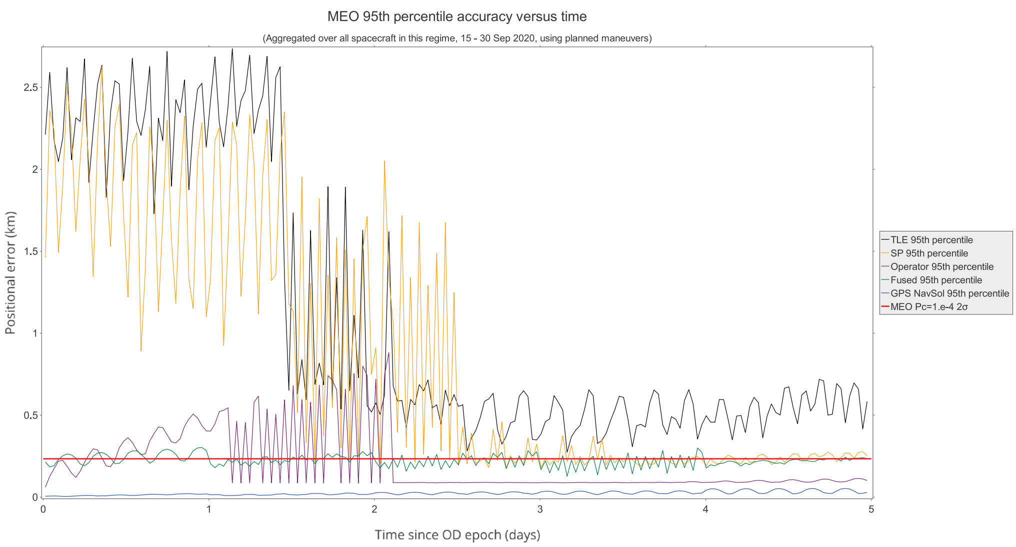

Fig. 53 MEO: 95th percentile positional accuracy versus sample accuracy requirement.

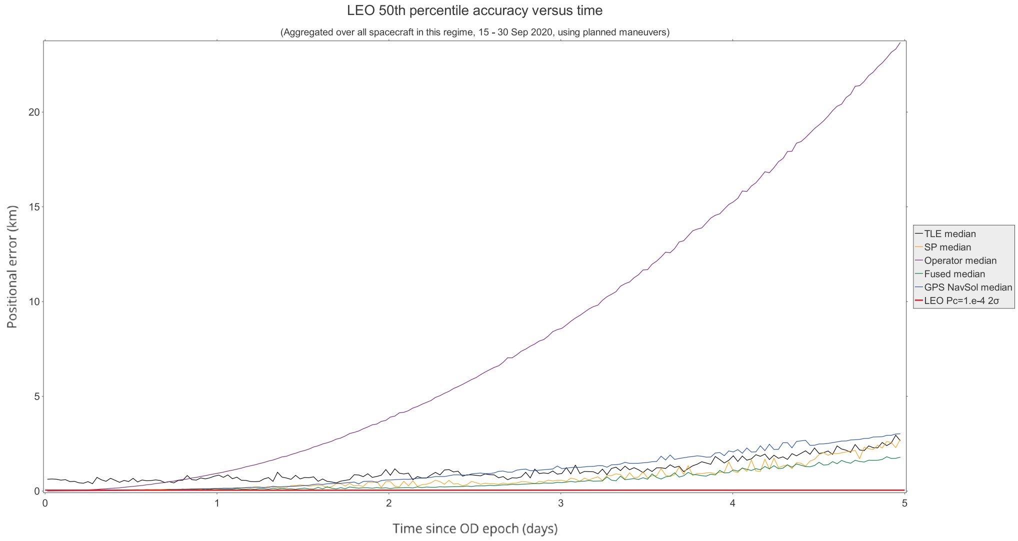

Fig. 54 LEO: 50th percentile positional accuracy versus sample accuracy requirement.

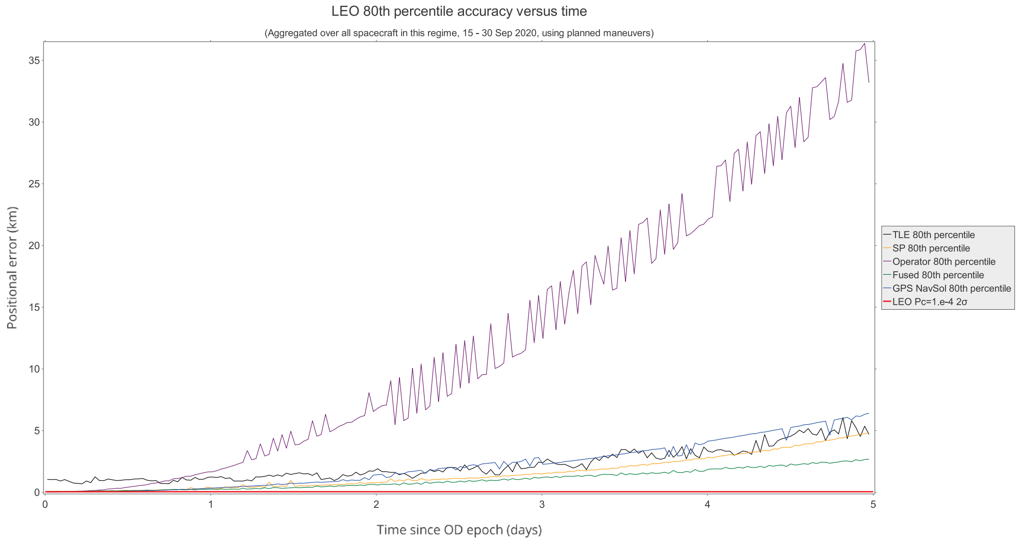

Fig. 55 LEO: 80th percentile positional accuracy versus sample accuracy requirement.

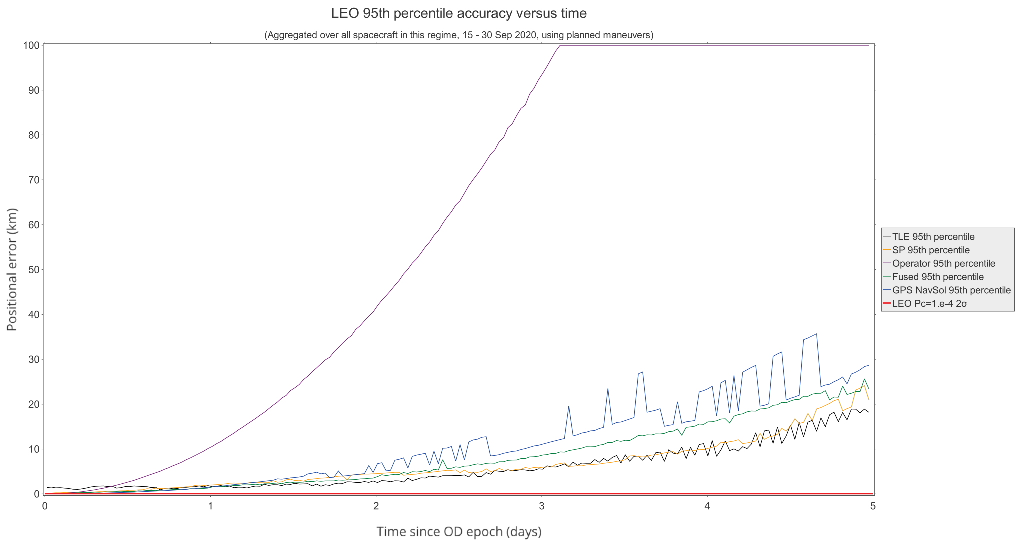

Fig. 56 LEO: 95th percentile positional accuracy versus sample accuracy requirement.

A3.2. Log-scale accuracy stats

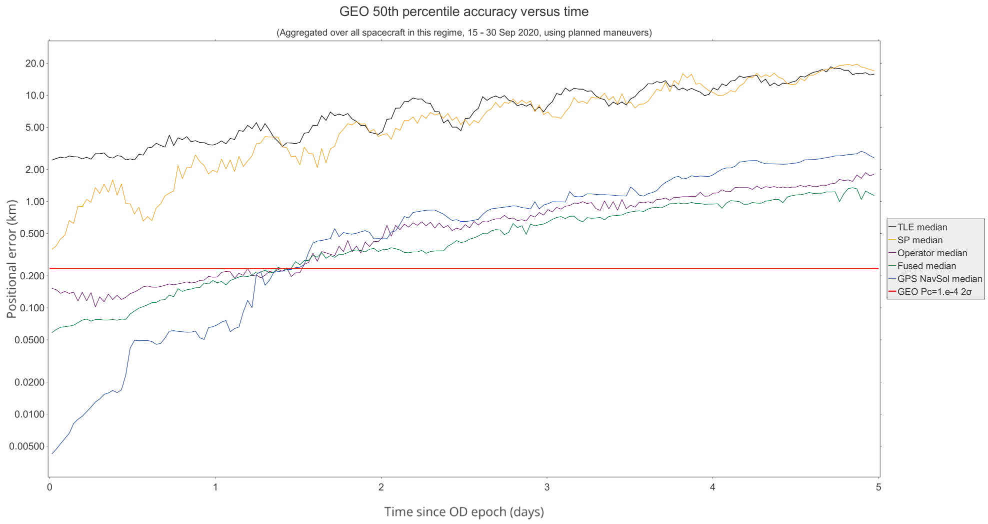

Fig. 57 GEO: 50th percentile positional accuracy versus sample accuracy requirement.

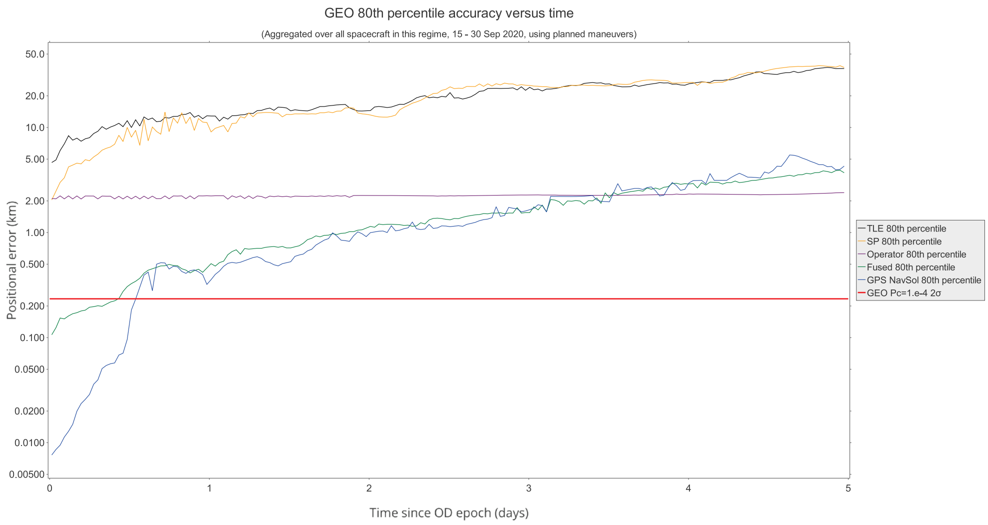

Fig. 58 GEO: 80th percentile positional accuracy versus sample accuracy requirement.

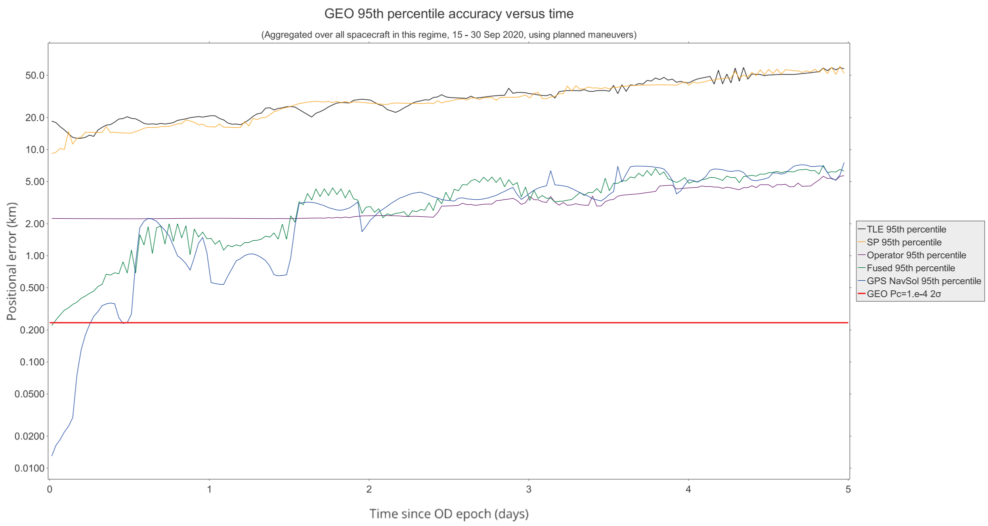

Fig. 59 GEO: 95th percentile positional accuracy versus sample accuracy requirement.

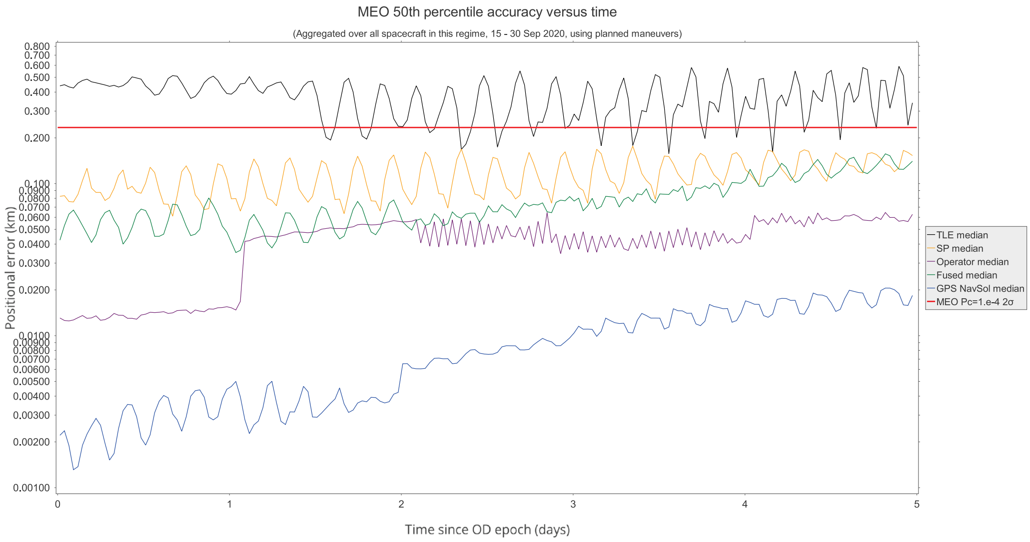

Fig. 60 MEO: 50th percentile positional accuracy versus sample accuracy requirement.

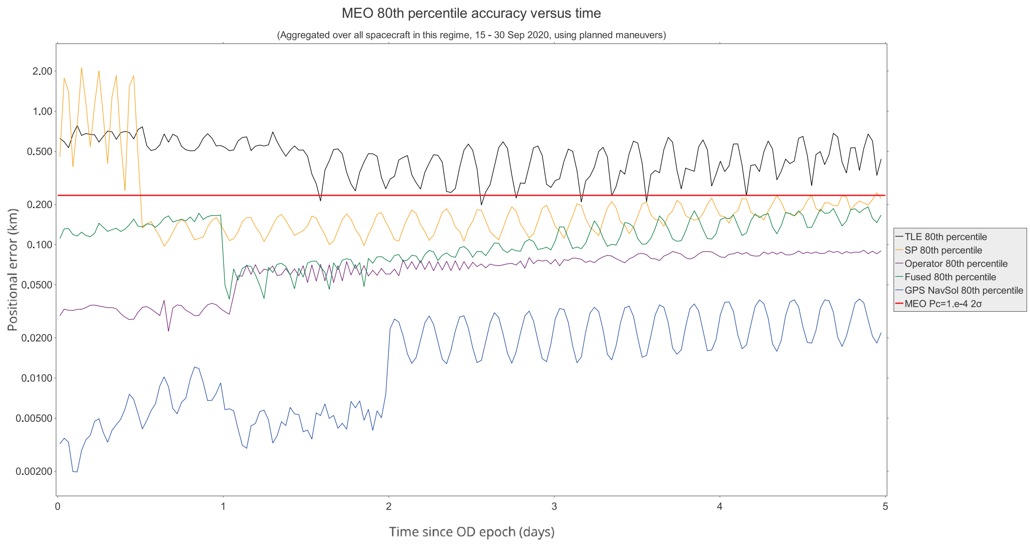

Fig. 61 MEO: 80th percentile positional accuracy versus sample accuracy requirement.

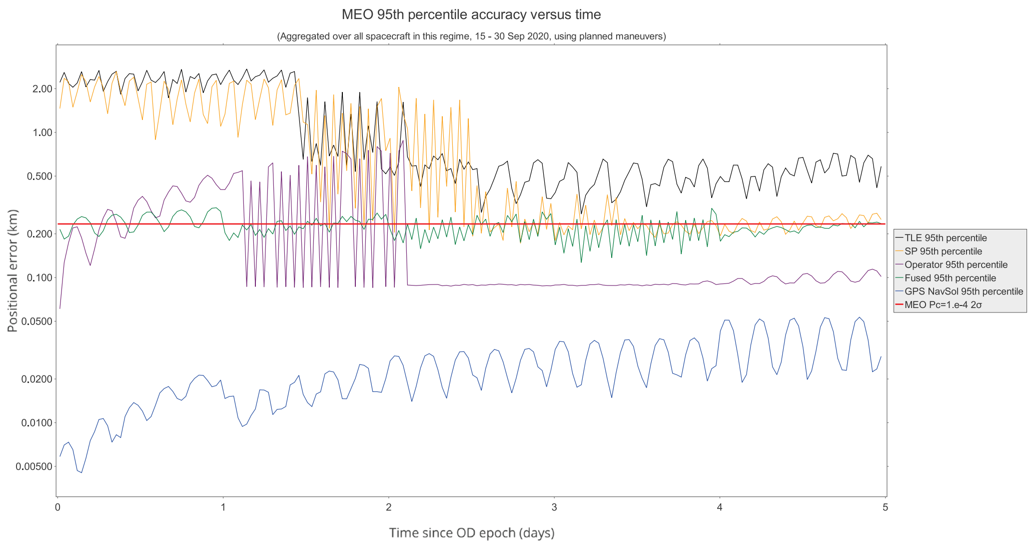

Fig. 62 MEO: 95th percentile positional accuracy versus sample accuracy requirement.

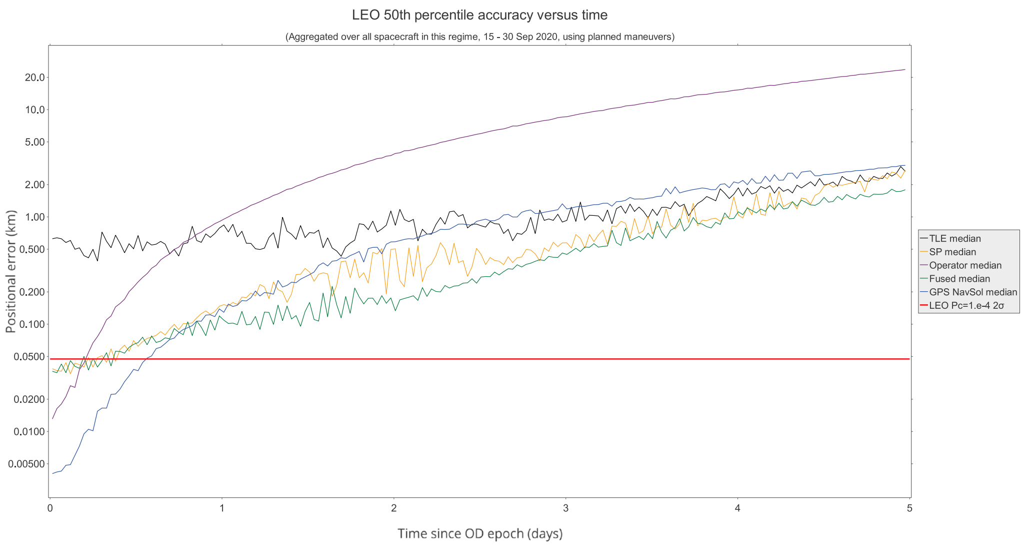

Fig. 63 LEO: 50th percentile positional accuracy versus sample accuracy requirement.

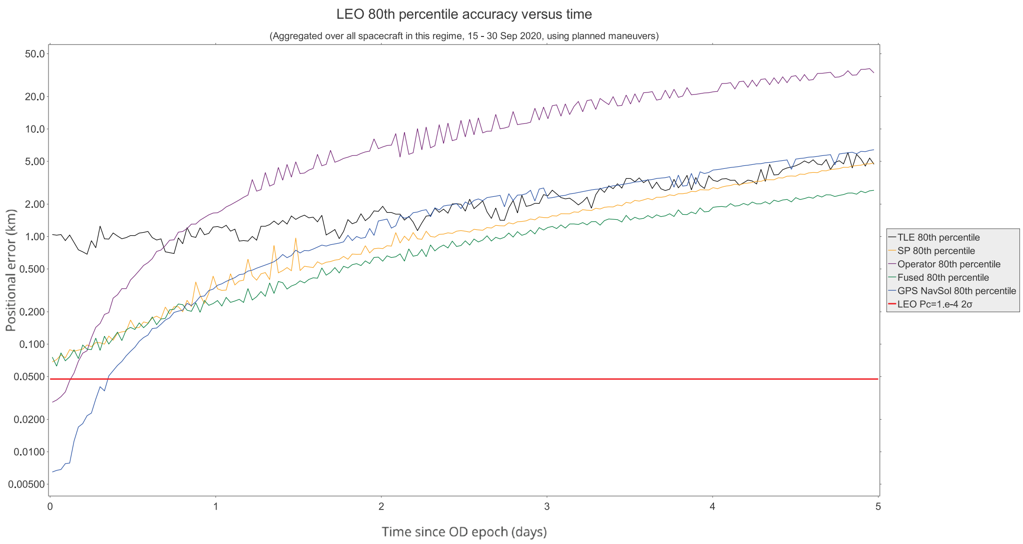

Fig. 64 LEO: 80th percentile positional accuracy versus sample accuracy requirement.

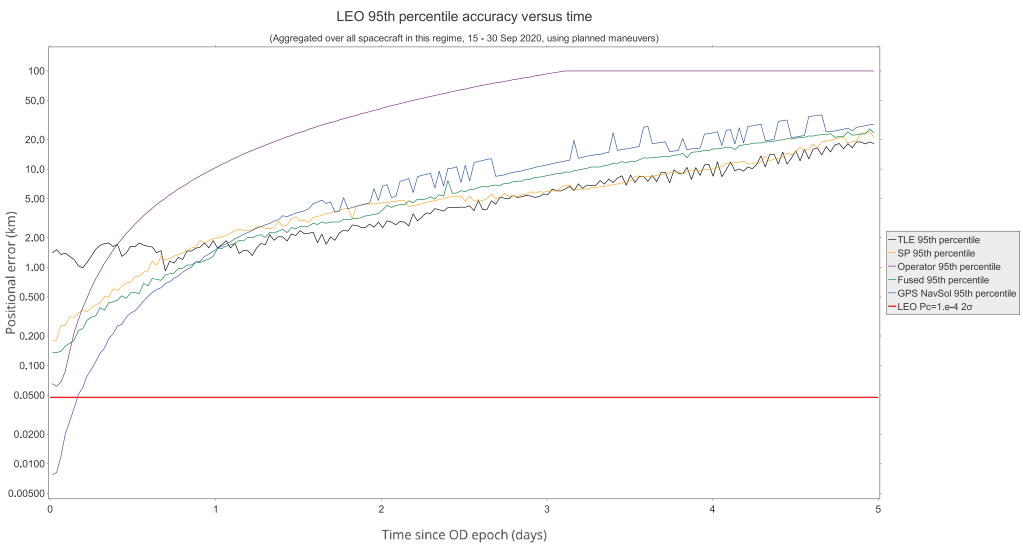

Fig. 65 LEO: 95th percentile positional accuracy versus sample accuracy requirement.

Appendix 4. LEOP Accuracy

This section provides the accuracy characterizations for the three SkySat satellites assessed during their Launch and Early Orbit Phase (LEOP).

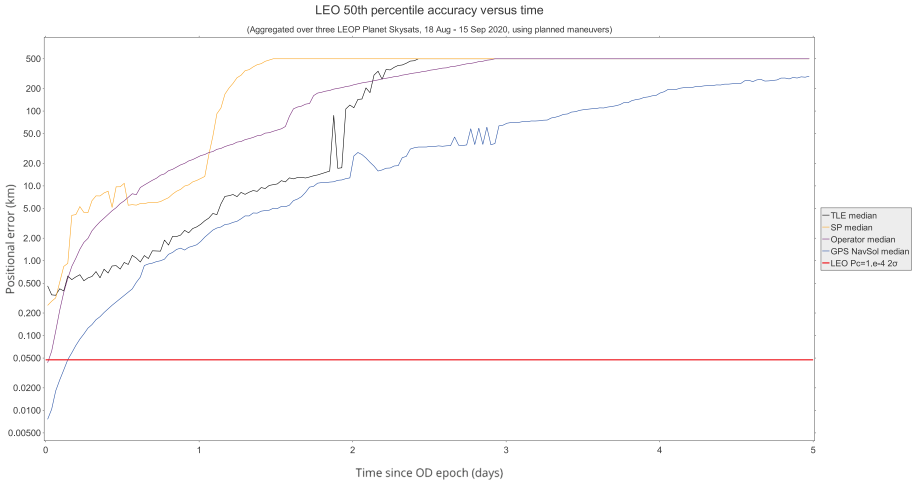

Fig. 66 Aggregate 50th percentile accuracy for 3 SkySats, 18 Aug – 15 Sept 2020.

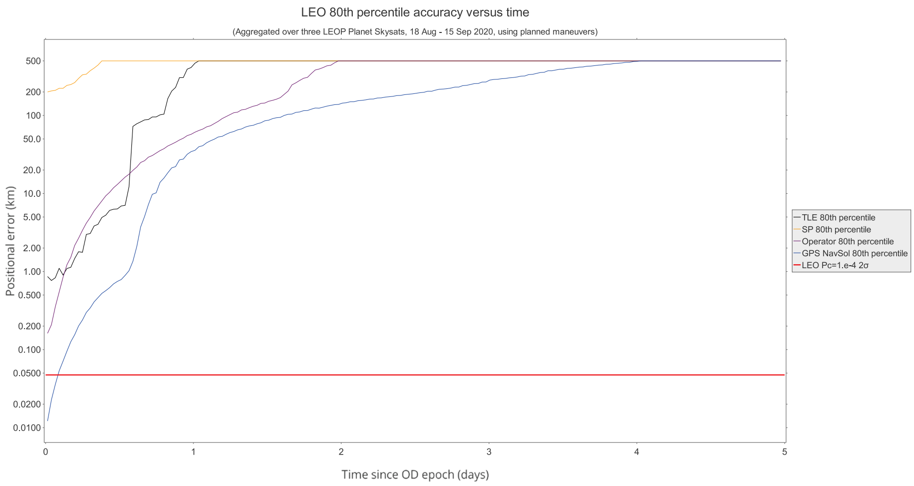

Fig. 67 Aggregate 80th percentile accuracy for 3 SkySats, 18 Aug – 15 Sept 2020.

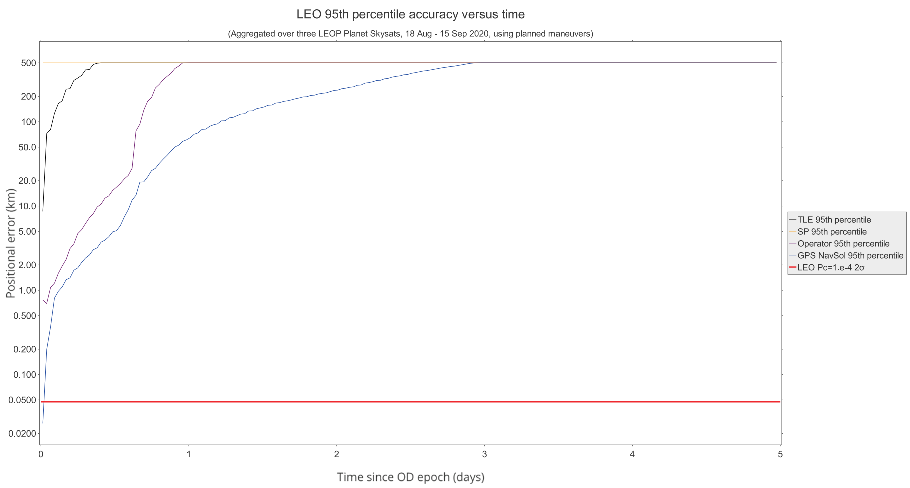

Fig. 68 Aggregate 95th percentile accuracy for 3 SkySats, 18 Aug – 15 Sept 2020.